ECD, a novel androgen receptor target promotes prostate cancer tumorigenesis by regulating glycolysis

Mohsin Raza[1#], Asher Rajkumar Rajan[1#], Benjamin B. Kennedy[1], Timothy E. Reznicek[1], Farshid Oruji[1], Sameer Mirza[1$], M Jordan Rowley[1], Carsten Stephan[5], Glen Kristiansen[6], Kaustubh Datta[2@], Bhopal C. Mohapatra[1*], Hamid Band[1, 3, 4*], and Vimla Band[1, 4*]

Department of [1]Genetics, Cell Biology and Anatomy, [2]Department of Biochemistry and Molecular Biology, [3]Eppley Institute for Research in Cancer, and [4]Fred & Pamela Buffett Cancer Center, University of Nebraska Medical Center, 985805 Nebraska Medical Center, Omaha, NE, [5]Department of Urology, Charité - Universitätsmedizin Berlin, Berlin, Germany and [6]Institute for Pathology, University Hospital Carl-Gustav-Carus, University of Technology, Dresden, Fetscherstrasse 74, D-01307 Dresden, Germany.

#Both authors contributed equally to this manuscript.

***Corresponding authors**: Vimla Band, PhD, Department of Genetics Cell Biology & Anatomy, University of Nebraska Medical Center, 985805 Nebraska Medical Center, Omaha, NE, 68198, USA. vband@unmc.edu; Phone: 402-559-8565. Hamid Band, MD, PhD, Eppley Institute for Research in Cancer, and Allied Disease, 985950 Nebraska Medical Center, Omaha, NE 68198-5950, USA; Email: hband@unmc.edu; Phone: 402-559-8572. Bhopal C. Mohapatra, Department of Genetics, Cell Biology, and Anatomy, University of Nebraska Medical Center 985805 Nebraska Medical Center, Omaha, NE 68198. Phone: 402-559-8543; E-mail: bmohapat@unmc.edu.

Current Addresses: [$]Department of Chemistry, College of Science, UAEU University, Al Ain, Abu Dhabi, U. A. E. [@] Department of Biochemistry and Molecular Biology, Massy Cancer Center, Virginia Commonwealth University, Richmond, VA, United States.

Running Title: ECD, an AR target gene, regulates glycolysis to promote PC oncogenesis.

Keywords: Androgens, androgen receptors, ecdysoneless (ECD), glycolysis, prostate cancer, oncogenesis, enzalutamide

Abstract:

Androgen receptor (AR)-mediated signaling is essential for PC tumorigenesis. In the TCGA database we observed a positive correlation between ECD and AR expression. Consistently, Dihydrotestosterone (DHT) treatment of PC cell lines increased ECD mRNA and protein levels, and AR knockdown (KD) reduced ECD expression. Bioinformatic analysis predicted three consensus androgen response elements in the ECD promoter, and DHT treatment increased AR occupancy at the ECD promoter, and enhanced ECD promoter activity. Enzalutamide treatment decreased ECD levels, and ECD knockout (KO) in PC cells reduced oncogenic traits, suggesting a functional role of ECD to maintain PC oncogenesis. ECD mRNA and protein are overexpressed in PC patient tissues, and its overexpression predicts shorter survival. Overexpression of ECD in PC cell lines enhanced the oncogenic traits *in vitro* and developed faster and larger highly proliferative xenograft tumors. RNA-seq analysis of mouse tumors revealed an increase in mRNA levels of several glycolytic genes. ECD associates with mRNA of key glycolytic genes and is required for their stability, consistent with our recent demonstration of ECD is an RNA binding protein. Higher glucose uptake and glycolysis was seen upon ECD overexpression in PC cells. Together, we demonstrate the role of a novel AR target gene ECD in PC tumorigenesis.

Introduction:

Prostate cancer (PC) is the second leading cause of cancer related adult males deaths [1]. Androgen receptor (AR) mediated signaling activated through binding of androgens is essential for PC tumorigenesis [2]. Initial androgen deprivation therapy is invariably followed by development of castration resistant PC (CRPC) [3]. AR inhibitors have proven effective but resistance to these inhibitors develops within 2-3 years, even though most such patients retain a functional AR that sustains tumor growth and spread [4, 5]. Thus, understanding of novel molecular pathways that sustain the AR-driven PC tumorigenesis could open novel approaches to therapy of AR-dependent PC.

Most solid tumors, including PC, exhibit metabolic reprogramming to cope with increased macromolecular synthetic, redox and energetic demands for increased oncogenic traits [6]. The hallmark of cancer cells, the Warburg effect, involves a switch to aerobic glycolysis instead of oxidative phosphorylation [7]. Increase in the rate of glycolytic flux has been reported during the late stage of high-grade primary PC, and CRPC, as well as PC with neuroendocrine differentiation [8, 9]. In addition, PC has been shown to maintain a unique androgen regulated metabolic profile with high rates of lipogenesis as well as oxidative phosphorylation [10]. While the role of glycolysis is well accepted across cancers, mechanisms that promote glycolysis in AR-dependent PC remain an area of active investigation. A unique property of prostate epithelial cells is that glycolytic metabolism sustains physiological citrate secretion and in early stages of PC, citrate is needed for oxidative phosphorylation and lipogenesis for tumor progression, however, in advanced and incurable CRPC, a metabolic shift towards choline, amino acid, and glycolytic metabolism takes over tumor progression [11]. Thus, inhibiting glycolysis in advanced PC provides a unique opportunity. Here, we identify ECD as a novel link between AR-dependent PC tumorigenesis by

24 modulation of glycolysis through its novel RNA binding role to stabilize mRNAs of key glycolytic
25 genes.

26 ECD is the highly conserved mammalian orthologue of *Drosophila* ecdysoneless (ECD)
27 gene [12]. *Ecd* in essential for mouse embryonic development and deletion of *Ecd* in $Ecd^{flox/flox}$
28 mouse embryonic fibroblasts (MEFs) led to G1 cell cycle arrest [13]. ECD plays a role in
29 mitigating endoplasmic reticulum stress through upregulation of GRP78 [14]. Previously, we have
30 shown that ECD contains a nuclear export signal and shuttles between the nucleus and cytoplasm
31 [15]. Notably, it interacts with several components of the mRNA spliceosome machinery, and
32 participates in pre-mRNA processing in both drosophila and mammalian cells [16, 17], as well as
33 in mRNA export in mammalian cells [18]. Our [19, 20] and others' studies have established that
34 ECD mRNA and protein are overexpressed in various solid cancers, and that ECD overexpression
35 (OE) plays a critical role in promoting tumorigenesis [21, 22]. Importantly, transgenic ECD OE
36 targeted to mouse mammary epithelium led to mammary epithelial hyperplasia and tumorigenesis
37 [23]. However, the role and regulation of ECD in PC tumorigenesis has remained unexplored until
38 this study.

39 Here, we establish that ECD is a novel AR target gene, and its' expression correlates with
40 AR expression. ECD expression is regulated by AR, through androgen-dependent AR recruitment
41 to the ECD promoter, and androgen treatment increased ECD promoter activity. Enzalutamide
42 treatment decreases ECD levels, as well as ECD KO decreases oncogenic traits, suggesting a key
43 role of ECD in PC oncogenesis. ECD mRNA and protein are overexpressed in PC patient tissues,
44 with ECD OE predicting short survival in PC patients. ECD OE enhanced *in vitro* oncogenic traits,
45 as well as *in vivo* tumorigenicity. Using RNA-seq analysis of xenograft tumors, RNA
46 immunoprecipitation analyses, and functional assays we demonstrate that ECD binds to and

47 stabilizes the mRNAs of key glycolytic genes to promote glycolysis. Thus, our studies identify a
48 novel AR target gene ECD and its function in promoting PC oncogenesis through regulation of
49 glycolysis.

50

51 **Results:**

52 **ECD expression in prostate cancer cells is regulated by androgen receptor.**

53 All PC are initially androgen-driven [24] and most remain dependent on androgen receptor
54 signaling even after castration-resistant [25], Given the connection of AR in PC, we analyzed
55 TCGA-prostate adenocarcinoma dataset and observed a significant positive correlation between
56 AR and ECD mRNA expression **(Fig. 1A)**. To test this *in vitro*, we used AR positive ECD
57 expressing prostate cancer cell lines (**Fig. S1A**): LNCaP (androgen-responsive, derived from a
58 lymph node metastasis of human prostatic adenocarcinoma), C4-2B (an androgen-independent
59 LNCaP subline isolated from bone metastasis in castrated mice [26], 22Rv1 (androgen responsive,
60 human prostate carcinoma cell line [27] and VCaP (androgen sensitive cells derived from vertebral
61 PC metastasis [28]. Despite differing androgen sensitivity, AR expression remains essential for
62 proliferation and survival in these cell lines [29-31]. Consistently, DHT dose-response **(Fig. 1B-**
63 **E, and Fig. S1B-E)**, as well as time-course analyses (**Fig. 1F-I, and Fig. S1H & I)** in four cell
64 lines LNCaP, C4-2B, 22Rv1, and VCaP cell lines showed ECD protein and mRNA levels
65 increased rapidly, plateaued at later time points and decreased towards the end of the time course.
66 Decreased at later time points is similar to other AR target genes, such as PSA, possibly due to
67 limited DHT due to its metabolism over longer time in charcoal-stripped serum [32]. Further, the
68 basal as well as DHT-induced increase in ECD protein levels were abrogated by siRNA KD of
69 AR, which was confirmed by anti-AR immunoblotting in LNCaP **(Fig. 1J)**, C4-2B **(Fig. 1K),**

70 22Rv1 **(Fig. S1J),** and VCaP **(Fig. S1K)** cells with or without the addition of exogenous DHT.
71 These results show that ECD expression in PC cell models is positively regulated by androgens
72 and dependent on the AR, suggesting the likelihood that ECD is transcriptionally regulated by AR.
73

74 **AR binds to the ECD promoter to regulate ECD expression, and Enzalutamide treatment**
75 **decreases ECD expression.**

76 Both androgens activated and constitutively active ARs function by binding to gene
77 promotors through defined androgen response elements (AREs) to regulate transcription of
78 downstream target genes [33]. Given that DHT induction, combined with AR dependence of *ECD*
79 mRNA expression, we examined the ECD promoter region for potential AR binding sites, using
80 three independent prediction tools, Pscan [34], EPD motif search tool [35] and de novo motif
81 discovery algorithm Motif Based Sequence analysis tool [36]. These analyses revealed three
82 potential androgen response elements (AREs) in the ECD promoter: nucleotides -698 to - 682 (site
83 1); -657 to -641 (site 2); and -640 to -624 (site 3) **(Fig. 2A & B)**. Indeed, chromatin
84 immunoprecipitation (ChIP) assays demonstrated specific occupancy of AR at the ECD promoter
85 (-712 to -565, encompassing all three sites) in all four, LNCaP, C4-2B, 22Rv1, and VCaP PC cell
86 lines compared to IgG control, with the occupancy significantly increased upon DHT treatment
87 **(Fig. 2C & D, and Fig. S2A & B)**. Next, we cloned a ~1,500 bp region encompassing the ECD
88 promotor region in a reporter construct upstream of secreted Gaussia Luciferase. PC cells
89 transduced with the ECD promotor Luciferase construct were left untreated or treated with DHT
90 for 3 hours, and secreted Gaussia Luciferase and alkaline phosphatase (SEAP; internal control)
91 activities were measured in the media. Notably, compared to basal reporter activity (Ctrl; first bar),
92 DHT treated cells expressing the Full length ECD promoter showed about 2.5-fold increase in

93 luciferase activity **(Fig. 2E & F, lane 2)**. Importantly, constructs with deletion of AREs either
94 alone or in combination showed progressive diminution of luciferase activity while the construct
95 with all three AREs deleted showed activity close to that of the control **(Fig. 2E & F, lanes 3-9).**
96 Collectively, our results identify ECD is an AR-regulated gene, with three functional ARE
97 elements in its promoter region that mediate androgen-induced AR-dependent ECD expression.

98 Based on a published report GSE 48403 [37] showed ECD mRNA expression was
99 decreased post-androgen-deprivation therapy as compared to pre-treatment **(Fig. 2G),** we treated
100 LNCaP, C4-2B, 22Rv1, and VCaP cell lines with different concentrations of Enzalutamide in the
101 presence of DHT. Notably, Enzalutamide treatment dose-dependently decreased ECD protein
102 levels in all four cell lines **(Fig. 2H & I, and Fig. S2C & D)**. Enzalutamide is reported to inhibit
103 AR binding to androgen and destabilize AR by dissociating it from the HSP90 complex, resulting
104 in reduced AR protein stability [38, 39], consistent with this, we observed a decrease in AR and
105 PSA, an AR target gene **(Fig. 2H & I, and Fig. S2C & D)**. Enzalutamide induced reduction in
106 ECD is at the transcriptional levels **(Fig. 2J & K, and Fig. S2E & F)**. Together, these results
107 conclusively demonstrate ECD is a novel AR target gene.

108

109 **ECD expression is required to sustain oncogenic traits of prostate cancer cells.**

110 Next, we engineered the androgen-dependent LNCaP and VCaP cell lines, as well as
111 androgen-independent C4-2B and 22Rv1 cell lines for doxycycline (Dox)-inducible CRISPR
112 knockout with two distinct guide RNAs (gRNA1 and gRNA2) against ECD. Dox-inducible
113 depletion of ECD in gRNA1/2 expressing cell lines compared to the non-targeted control (Cas9-
114 NTC) was observed **(Fig. 3A, and Fig. S3A & B).** Analysis of colony forming capacity as a
115 measure of cell growth demonstrated that ECD depletion led a significant decrease in PC cell

116 proliferation compared to NTC **(Fig. 3B & C)**. Further, ECD depletion in comparison with NTC
117 exhibited a significant decrease in oncogenic traits, such as tumorsphere forming ability **(Fig. 3D**
118 **& E, and Fig. S3C & D),** a measurement of the stem cell ability of tumor cell lines [40], anchorage
119 independent growth using the soft agar colony forming assay **(Fig. 3F & G, and Fig. S3E & F)**,
120 three-dimensional growth in Matrigel **(Fig. 3H & I, and Fig. S3G & H),** cell migration **(Fig. 3J**
121 **& K, and Fig. S3I & J),** as well as tumor cell invasion **(Fig. 3L & M, and Fig. S3K & L).** Given
122 that AR is a primary driver of prostate carcinogenesis, and ECD being a transcriptional target of
123 AR, we investigated the extent to which AR-mediated induction of ECD contributes to AR-driven
124 oncogenic processes. To address this, we performed siRNA-mediated knockdown of AR and
125 rescue with ECD in two PC cell lines LNCaP and C4-2B (**Fig. S4A & B)**. Following knockdown
126 and rescue, we conducted soft agar colony formation and Matrigel organoid formation assays to
127 assess oncogenic potential. These experiments revealed that overexpression of ECD partially
128 mitigated the suppressive effects of AR knockdown on soft agar colony (**Fig. S4C-E)** and organoid
129 formation (**Fig. S4F-H)**. These results highlight ECD as a potential downstream target of AR
130 signaling in prostate cancer. Taken together, these results establish a critical role of ECD
131 expression in sustaining the oncogenic traits of PC cells.
132
133 **ECD protein is overexpressed in prostate cancer tumor tissues, and its overexpression**
134 **predicts shorter patient survival.**
135 To assess the expression levels of ECD in primary PC tumor samples, we carried out IHC
136 analysis of a PC tissue microarray (TMAs) comprising of 522 patient samples with available
137 clinical, pathological and survival data using a previously validated anti-ECD antibody [13]. PC
138 samples showed a range of ECD IHC staining. The intensity of staining was expressed as a

139 semiquantitative scoring system: negative = 0, low = 1, moderate = 2 and High =3. Frequency
140 and percentage of patients in each score were assigned and listed (**Fig. 4A**). Based on the intensity
141 of staining, the patients were grouped into ECD-low (staining intensity of 0 or 1) and ECD-high
142 (staining intensity of 2 or 3) groups; representative examples of low IHC staining of hyperplastic
143 tissue, and PC tumor samples low vs. high ECD IHC staining are presented **(Fig. 4B & C)**. Overall,
144 ECD protein was overexpressed in tumor samples of ~40% of PC patients **(Fig. 4D)**. Kaplan Meier
145 analysis showed that OE of ECD protein correlated with shorter overall survival (p=0.024) **(Fig.**
146 **4D)**. The case processing summary table describes the number of events where patient outcome
147 was available, censored are the patients where outcome was unknown, and number of patients used
148 for survival analysis with ECD-low (0&1 score) and ECD-high (2&3 score) (**Fig. 4E)**. Multivariate
149 survival analysis was performed using Cox regression model to evaluate the influence of ECD
150 expression, tumor pT stage, Gleason grade, R-status, age, and pre-operative PSA, on a patient's
151 overall survival. Patients' overall survival was significantly dependent on ECD expression
152 (relative risk, RR= 1.69, p= 0.02), tumor pT stage (RR= 3.12, p= 0.0), Gleason grade (RR=2.4,
153 p=0.009), and R-status (RR=1.66, p=0.03 whereas age and pre-operative PSA failed significance
154 **(Table S1).** This analysis independently confirmed the high expression of ECD as a poor
155 prognostic marker, with a significantly elevated relative risk. In addition, analysis of two publicly
156 available mRNA expression datasets (GSE32269 & GSE35988) revealed *ECD* mRNA
157 overexpression in PC tissues as compared to normal prostate **(Fig. S5A & B).** Kaplan-Meier
158 analysis of The Cancer Genome Atlas (TCGA) dataset of 484 mixed prostate adenocarcinoma
159 samples (2022-v32) using the R2 Genomics platform showed that high ECD mRNA was
160 associated with shorter patient survival **(Fig. 4F)**. Collectively, our results show that ECD mRNA
161 and protein levels are increased in a significant subset of PC tumor samples, and that ECD OE

162 correlates with negative prognostic features and shorter survival of patients, suggesting that ECD
163 OE may promote PC tumorigenesis.
164
165 **ECD overexpression in PC cells promotes the *in vitro* oncogenic traits and *in vivo***
166 **tumorigenesis.**
167 Next, we established stable ECD-OE PC cell lines LNCaP (hormone sensitive), its
168 derivatives C4-2B (hormone insensitive), and 22Rv1 (hormone insensitive). Overexpression of
169 ECD is observed in all three LNCaP **(Fig. 5A),** C4-2B **(Fig. S6A),** and 22Rv1 **(Fig. S6B)** cell lines**.**
170 While there were no significant differences in proliferation of vector vs ECD-OE PC cell lines
171 when measured in two-dimensional culture **(Fig. S6C-E),** a significant increase in anchorage
172 independent growth in soft agar **(Fig. 5B & C, and Fig. S6F-I)**, as well as in three-dimensional
173 Matrigel growth **(Fig. 5D & E, and Fig. S6J-M)** was seen in three (LNCaP, C4-2B, and 22Rv1)
174 ECD-overexpressing vs. vector control cells. Notably, ECD-OE LNCaP cells remain hormone
175 sensitive like control cells **(Fig. S6N).**
176 To assess the impact of ECD OE on *in vivo* oncogenesis of PC cells, we introduced a
177 mCherry-luciferase reporter into vector control and ECD-overexpressing LNCaP cells and
178 subcutaneously injected these in the dorsal flank region of 8-weeks old male athymic nude mice.
179 Tumor growth was monitored twice a week using calipers and weekly using bioluminescence
180 imaging. Compared to the time course of tumor growth in mice implanted with control cells, those
181 implanted with ECD-overexpressing cells developed more tumors that appeared earlier and grew
182 to be significantly larger (**Fig. 5F-J, Table S2).** IHC staining of tumor sections confirmed the
183 overexpression of ECD in ECD-OE tumors **(Fig. 5K)**. H&E-stained tumor sections showed that
184 ECD-OE tumors had more necrosis **(Fig. 5K)**, a characteristic of aggressive tumors [41]. Finally,

185 ECD-OE tumors showed increased Ki-67 staining **(Fig. 5K)**, a marker of tumor cell proliferation
186 [42]. Together, the combination of *in vitro* and *in vivo* analyses demonstrates that ECD OE
187 enhances the tumorigenic behavior of PC cells.
188
189 **ECD overexpression in prostate cancer cells upregulates the glycolysis pathway.**
190 To explore how ECD OE promotes the tumorigenic behavior of PC cells, we conducted
191 RNA-seq analysis of xenograft tumors formed by ECD-overexpressing vs. Vector-expressing
192 LNCaP cells followed by bioinformatics analyses. Principal component analysis (PCA)
193 demonstrated the distinct clusters of the four each of the two types of tumors **(Fig. 6A**). Based on
194 a log fold change >1 and false discovery rate (FDR) of <0.05, we found 520 differentially
195 expressed genes (DEGs) in ECD-overexpressing compared to vector control tumors. Gene set
196 enrichment analysis (GSEA) using the hallmark gene sets showed a significant upregulation of
197 hypoxia, glycolysis, angiogenesis, myogenesis, apical junctions, TNFα signaling via NFkB and
198 mTORC1 signaling in ECD-OE tumors compared to vector control tumors (**Fig. 6B & C**). These
199 signaling pathways are well-known to be upregulated in aggressive prostate cancers [43-45].
200 Among the genes upregulated in ECD-OE LNCaP tumors were key glycolytic pathway genes
201 (*ALDOA, LDHA, PKM, PGK1, HK1, HK2, ENO1*), Epithelial to Mesenchymal Transition (EMT)
202 related genes (*VIM, SNAI1, TWIST2, TGFb1, TGFb2, HMGA2),* invasion and migration associated
203 genes (*MMP2, MMP13, MMP14, MMP15* and *MMP24*), and genes associated with Notch
204 signaling (NOTCH1, NOTCH2, NOTCH3 and NOTCH4), FGFR signaling (SPRY2, FGFR1)
205 [44], and a previously identified aggressive prostate cancer signature gene set (*CCND2, RNF19A,*
206 *DPP4* and *PRKDC*) [45] (**Fig. 6D**). In addition, ECD-OE tumors exhibited increased expression
207 of neuro-endocrine prostate cancer (NEPC) related genes (*SYP*, *EZH2, ENO2, NRP2, NCAM1 and*

208 *SOX2)*, a features of aggressive metastatic castration resistant PC (mCRPC) [46] (**Fig. 6D**). qRT-
209 PCR analysis of mRNA isolated from xenograft tumors and *in vitro* cultured LNCaP cell lines
210 validated the significant upregulation of glycolytic genes *HK2, LDHA and PKM2* (**Fig. 6E-G**) and
211 NEPC related *SYP, NCAM1* and *ENO2* **(Fig. S7A & B)** in ECD-OE group compared to vector
212 control. To further validate our qRT-PCR analysis of glycolytic mRNAs at protein level, we
213 performed IHC analysis of vector and ECD-OE xenograft tumors and observed higher staining of
214 HK2 and LDHA in tumor sections of ECD-OE LNCaP xenografts, as compared to controls (**Fig.**
215 **S8)**.

216 Together, these results suggested the upregulation of glycolysis as a potential mechanism
217 of ECD-promoted oncogenesis, consistent with the previously identified role of ECD in promoting
218 glycolysis related gene expressions in mammary tumors of *ECD*Tg mice [23].

219 Given our'[18, 19, 47] and others' recent findings that ECD regulates various aspects of
220 mRNA biogenesis [48] and our recent findings that ECD is a RNA binding protein [47], we
221 examined if ECD directly binds to and regulates glycolytic genes. LDHA and PKM2 were among
222 the ECD interacting mRNAs identified through our recent analyses using enhanced crosslinking
223 and immunoprecipitation (eCLIP) assay [47]. Using an RNA immunoprecipitation (RIP) assay,
224 we found that *LDHA*, *PKM2* and *HK2* mRNAs were associated with ECD in both LNCaP **(Fig.**
225 **7A)** and C42-B **(Fig. 7B)** cell lines. Next, we analyzed the stability of these mRNAs in control vs.
226 ECD-overexpressing cells by determining mRNA half-lives following treatment with
227 actinomycin-D. These analyses revealed significantly longer (1.5 to 2-fold) half-lives of *PKM2*,
228 *HK2* and *LDHA* in ECD-overexpressing vs. control LNCaP **(Fig. 7C-E)** and C4-2B **(Fig. 7F-H)**
229 PC cells, determining that ECD binds to and stabilizes the mRNAs of key glycolytic genes.

230 To functionally link the upregulation of glycolytic gene mRNA levels upon ECD OE to

231 glycolysis, a Warburg effect [49], we measured glucose uptake and glycolytic rates. Indeed, there
232 was a significant increase in glucose uptake in ECD-OE LNCaP (**Fig. 8A**) and C4-2B (**Fig. 8B**)
233 cell lines as compared to vector expressing cells. To directly assess the impact on glycolysis, we
234 conducted Seahorse XFe glycolytic rate assays to determine the proton efflux rate (PER) from
235 glycolysis (GlycoPER) and extracellular acidification rate (ECAR) as readouts of glycolysis.
236 Notably, the PER (**Fig. 8C & D**) and ECAR (**Fig. 8E & F**), measured in the presence of rotenone
237 (Rot) and antimycin A (AA) to inhibit mitochondrial respiration, were increased in ECD-OE cells
238 compared to vector cells. Additionally, ECD-OE cells showed increased levels of basal glycolysis
239 (**Fig. 8G & H**) as well as of glycolytic reserve/compensatory glycolysis (**Fig. 8I & J**) after adding
240 2-Deoxy-D-glucose (2-DG) compared to their vector controls. Further, cellular oxygen
241 consumption rate (OCR) was increased in ECD-OE PC cells relative to their controls **(Fig. S9A**
242 **& B)**. Since increased glycolysis is often associated with enhanced glycogen synthesis [6], we
243 performed Periodic Acid–Schiff (PAS) staining to assess glycogen deposition, [50] along with
244 IHC staining for glycogen synthase 1 (GYS1) and glycogen phosphorylase (PYGB), key enzymes
245 involved in glycogen metabolism,[50] in tumor sections from Vector and ECD-OE LNCaP
246 xenografts. Notably, we observed OE of ECD increased glycogen synthesis and metabolism, as
247 demonstrated by higher staining intensities of PAS **(Fig. S10A)**, GYS1 and PYGB **(Fig. S10B)**.
248 These results demonstrate that ECD OE in PC cells increases the expression of key glycolytic
249 genes through binding to and stabilization of their mRNAs to promote the Warburg effect.
250

251 **Discussion:**

252 While androgen signaling through AR is universally accepted as an early driver of prostate
253 tumorigenesis with well-established targeting agents, androgen and AR directed therapies

254 eventually fail in most patients [51]. Metabolic reprogramming represents a key molecular
255 determinant of the aggressive behavior of PC and therapeutic resistance, with enhanced glucose
256 utilization through aerobic glycolysis (Warburg effect) as a major factor [49]. Molecular pathways
257 that link AR signaling and glycolytic metabolism in PC are of interest as these are potential
258 biomarkers, as well as for therapeutic targeting in conjunction with AR directed therapies. Here,
259 we identify the Ecdysoneless (ECD) protein as a novel link between AR signaling and promotion
260 of glycolysis and demonstrate that ECD, which is overexpressed in >40% of PC patient tumors
261 and predicts shorter survival, is an AR-responsive target gene whose increased expression
262 promotes glycolysis through ECD binding to glycolytic gene mRNAs to enhance their stability.
263 Our studies elucidate a novel mechanism to promote metabolic reprogramming and tumorigenesis
264 in PC and raise the possibility of glycolysis pathway co-targeting with AR in ECD-OE PC.

265 AR-mediated signaling is a critical element of the early progression of all PCs and remains
266 an oncogenic driver in most late-stage PCs [48]. Our comprehensive analysis establishes that ECD
267 OE is directly regulated by AR signaling. We found a strong positive correlation between AR and
268 ECD mRNA expression levels across PCs (TCGA-PRAD dataset) **(Fig. 1A)** and cell-based
269 analyses of PC cell lines showed a dose- and time-dependent upregulation of ECD mRNA and
270 protein levels by exogeneous androgen treatment of PC cells **(Fig. 1B-I)** with siRNA KD
271 demonstrating a requirement of AR for basal as well as androgen-stimulated ECD expression **Fig.**
272 **1J & K**),. Direct evidence for ECD as a novel androgen-responsive AR target gene in PC was
273 provided by ChIP **(Fig. 2A-D)** that established the potential AREs identified by in-silico analysis
274 of the ECD promoter to be authentic AR binding sites and mutational analyses of the three AREs
275 using a luciferase reporter assay **(Fig. 2E & F)** demonstrated their combined requirement for
276 androgen-induced ECD expression. Consistently, treatment of PC cell lines with anti-androgen

277 Enzalutamide decreased ECD levels **(Fig. 2H-K)**. Further the role of ECD in PC was established
278 by genetic loss as well as gain of function approaches in PC cell line models. Inducible ECD KO
279 led to a marked reduction in key *in vitro* oncogenic traits **(Fig. 3A-M)**.

280 While ECD plays a physiological role in cell cycle progression and ER stress mitigation,
281 and its overexpression correlates with poor prognosis and shorter survival in breast, pancreatic
282 and gastric cancers [21, 22], any role and regulation of ECD in PC has remained unexplored. Our
283 IHC analyses of a large cohort of PC patient tumors using a well-authenticated anti-ECD
284 monoclonal antibody [52], showed ECD OE in nearly 43% of PC cases and such overexpression
285 specified shorter patient survival (**Fig**. **4A-E**). Analysis of publicly available TCGA PC
286 adenocarcinoma dataset demonstrating shorter survival of PC patients with higher ECD mRNA
287 expression **(Fig. 4F)** lend further support to our IHC results. Notably, high ECD OE was associated
288 with key bad prognostic indicators like higher Gleason score, advanced tumor stage and positive
289 resection margins **(Table S1)**. Thus, ECD OE emerges as a novel biomarker of poor prognosis and
290 shorter patient survival in PC.

291 These results support a novel mechanism whereby AR signaling induces the upregulation
292 of ECD expression in PC as one pro-oncogenic pathway. It is noteworthy that while we and others
293 have reported the upregulation of ECD expression in other cancers, the mechanisms responsible
294 for such overexpression remain unknown. Given the androgen/AR mediated upregulation of ECD
295 expression in PC identified here, it will be of great interest to assess the potential regulation of
296 ECD OE across cancers through other nuclear hormone receptors, especially in hormonally
297 regulated malignancies. Notably, the AR requirement for ECD OE was observed in an androgen-
298 dependent as well as an androgen-independent PC cell line model, suggesting that AR signaling
299 rather than exogenous androgen requirement is a key determinant of ECD OE in PC as significant

300 subsets of CRPCs are AR-independent [49]. Intriguingly, elevated levels of ECD are observed in
301 the AR-negative PC cell line PC3 (**Fig. S1A**), indicating that ECD regulation may not be solely
302 dependent on AR signaling. The possibility remains that ECD expressions in AR-negative PC may
303 be regulated by alternate steroid hormone receptor signaling pathways, such as those mediated by
304 glucocorticoid receptors (GR). Literature suggests that hormone responsive elements (HREs) are
305 similar to androgen response element (ARE) [53], and AR-negative PC often exhibit higher GR
306 expression [54]**.**. Future studies utilizing both AR-positive and AR-negative PC will help
307 determine the role of ECD through GR-mediated signaling.

308 Besides emerging as a correlative biomarker of aggressive PC, our studies clearly
309 demonstrate that ECD OE is biologically important in promoting the tumorigenic behavior of PC
310 cells **(Fig. 5A-E, and Fig. S6).** Notably, both vector and ECD-OE PC cells remain hormone
311 responsive for their proliferation **(Fig. S6N)**. Importantly, ECD OE imparted a more aggressive *in*
312 *vivo* tumorigenic phenotype with earlier growth of xenografted tumors, significantly larger tumors
313 (**Fig 5F-J**), and higher levels of Ki-67 staining and necrotic lesions indicative of hyper-
314 proliferative and rapidly growing aggressive tumors (**Fig. 5K**), consistent with known association
315 of hyperproliferation and necrosis with aggressive prostate tumors in patients [55]. Thus, like the
316 role of ECD OE in other cancers such as breast cancer [23], its overexpression appears to propel
317 PC towards increased aggression. We note that while our studies in established PC cell lines clearly
318 reveal the impact of ECD OE to promote tumorigenic phenotype, our studies do not address any
319 potential role of ECD OE in early malignant transformation driven by androgen-AR axis. In our
320 previous studies using immortalized mammary epithelial cell models, ECD OE alone did not
321 impart a tumorigenic phenotype [56]. However, since ECD plus mutant RAS co-overexpression
322 in immortal mammary epithelial cells promoted full tumorigenesis [56], and transgenic

323 overexpression of ECD in the mammary epithelium led to hyperplasia and late-onset tumor
324 induction [23], incorporation of ECD transgene or tissue-specific ECD KO genetic models of
325 prostate tumorigenesis should help assess a potential early pro-tumorigenic role of ECD in PC.

326 Our mechanistic studies provide a plausible explanation for the pro-oncogenic role of ECD
327 OE in PC. Our RNA-seq analyses identified a potential role of ECD OE in upregulating the mRNA
328 levels of key glycolytic genes, *HK2, LDHA* and *PKM2* **(Fig. 6)**. Consistent with our recently
329 established biochemical function of ECD as an RNA-binding protein [47], these mRNAs are
330 physically associated with ECD **(Fig. 7A & B)** and ECD OE enhances their stability **(Fig. 7C-H).**
331 A significant increase in glucose uptake (**Fig. 8A & B**) and glycolysis measured with Seahorse
332 glycolytic assays (**Fig. 8C-J**) directly established that the increased expression of glycolytic gene
333 mRNAs upon ECD OE translates into function of ECD in glycolysis. Furthermore, IHC staining
334 of ECD-OE LNCaP tumor xenografts showed higher expression of LDHA and HK2 (**Fig. S8**),
335 along with increased Periodic Acid Schiff (PAS) staining, and an increase level of GYS1 and PYGB
336 **(**proteins involved in glycogen metabolism) (**Fig. S10A & B**) further underscoring the role of ECD
337 to regulate glucose and glycogen metabolism. Thus, we posit that increased expression of ECD in
338 PC, initiated by androgen-AR signaling, serves as one mechanism to promote a glycolytic switch
339 to enhance the aggressiveness of PC. This mechanism is consistent with our analyses of ECD
340 transgene driven mammary tumors, which also exhibited an upregulation of glycolysis enzyme
341 mRNAs and increased glucose uptake [23]. A linkage of ECD OE to increased glycolysis as a
342 mechanism to enhance PC tumor aggressiveness is also consistent with prior studies that have
343 demonstrated a key role of aerobic glycolysis in promoting cell survival [57], metastasis [58] and
344 drug resistance in PC [59]. While our studies suggest the ECD OE as a potential positive regulator
345 of glycolysis in >40% of prostate tumors, clearly other mechanisms are likely to play a role either

346 concurrently with ECD OE or in patients without ECD OE. Notably, AR signaling is known to
347 control glycolysis directly in PC, [60] however other mechanisms like aberrant FGFR tyrosine
348 kinase signaling [61] and activation of Wnt/β-catenin signaling [62] have also been linked to
349 enhanced glycolysis in PC. Future studies will be needed to assess how ECD OE may synergize
350 with other mechanisms that promote glycolysis. Additional investigations are needed to elucidate
351 whether ECD, as an RNA-binding protein, and regulator of RNA splicing contributes to splicing
352 modulation of glycolytic genes, to further enhance glycolytic activity.

353 In conclusion our work reveals ECD as a novel androgen-regulated AR target gene and
354 demonstrates that ECD OE, a feature of >40% PC patients, promotes PC tumor aggressiveness
355 through upregulation of glycolysis. Our findings open the possibility of exploring glycolysis-
356 targeted therapeutic approaches for PC patients with high ECD expression. These results support
357 oncogenic role of ECD in both hormone dependent and hormone independent AR-expressing
358 prostate cancer.

359

360 **Materials and Methods:**

361 **Antibodies and reagents**

362 Antibodies: anti-AR (Invitrogen cat # MA5-13426), β-actin (Sigma cat # A5441), Ki67
363 (Abcam cat # ab16667), anti-PYGB (Proteintech cat # 12075-1-AP), anti-LDHA (R&D cat #
364 MAB9158), anti-HK2 (Abcam cat #ab209847), anti-GYS1 (ThermoFisher cat # 10566-1-AP),
365 anti-ECD antibody generated by us has been described previously [13]. 5α-Dihydrotestosterone
366 solution (Millipore Sigma cat # D-073), Chemiluminescence signals were detected by (ECL Plus;
367 Amersham-Pharmacia cat # NEL-105001EA) and Matrigel (Coring Cat # 356230), and Isoflurane
368 (cat # 502017) from MWI Animal Health.

369

370 **Cell lines and medium.**

371 PC cell lines LNCaP, C4-2B, 22Rv1, VCaP, PC-3 and HPV18 immortalized prostate
372 epithelial cells (RWPE-1) were obtained from the American Type Culture Collection (ATCC).
373 Cancer cell lines were maintained in complete RPMI medium with 10% fetal bovine serum [63]
374 and RWPE-1 was cultured in keratinocyte growth medium (KGM Bullet Kit, Lonza) [19]. For
375 androgen deprivation experiments, cells were cultured in phenol red-free complete RPMI medium
376 supplemented with 10% charcoal stripped FBS (cat # S11650 Atlanta Biologicals). Lenti-X 293T
377 cell line used for lentiviral packaging was from Takara Bio (cat # 632180) and cultured in complete
378 DMEM medium [63]. Cells were cultured in a humidified atmosphere with 5% CO_2 at 37°C. Cell
379 lines were regularly evaluated for mycoplasma and continuously cultured for no more than 3
380 months.

381

382 **Chromatin Immunoprecipitation assay.**

383 Cells grown in charcoal stripped medium and were treated with DHT for 3 h, washed with
384 PBS and treated with 1% formaldehyde for 10 min to crosslink protein-DNA complexes. Cells
385 were rinsed and processed for ChIP with control IgG (Abcam, cat # ab172730) or anti-AR antibody
386 (Abcam, cat # ab185913). The following PCR Primers were used to determine the enrichment:
387 ECD AR Binding site Forward primer -TTAATTCTGGGATCTTTATCTGTAG; ECD AR
388 Binding site Reverse primer- GGCTCCAGGAAAGTGCTCACTTGAC. Real- time PCR
389 quantification was performed in triplicates using SYBR Green PCR master mix (Applied
390 Biosystems cat # 4309155). AR Binding percentage was calculated post normalization against
391 IgG.

392

393 **Luciferase-promoter reporter assays.**

394 The promoter sequences of GAPDH (Genome=hg38;chr12+: 6533244-6534713;
395 TSS=6534517; Upstream=1273, Downstream=196; Length=1470), and wildtype (WT) ECD
396 (Genome=hg38;chr10-:73169381-73167884; TSS=73168095; Upstream=1286,
397 Downstream=211; Length=1498) or its predicted AR binding site deletion mutants (Details in
398 **Table S3**) were synthesized and cloned upstream of the Gaussia luciferase in the lentiviral pEZX-
399 LvPG04 vector (sequence-confirmed constructs were custom-made by Genecopoeia; cat#
400 HPRM35342-LvPG04-WT, GAPDH-LvPGO4). The ECD promoter mutants and the sequences
401 deleted from TSS are listed in **Table S3**. The reporter constructs were introduced into LNCaP and
402 C4-2B cell lines using lentiviral supernatants. For promotor luciferase experiments, transduced
403 cells were cultured in charcoal stripped serum containing medium for 5 days and then treated with
404 100 nM DHT for 3 h. Post treatment, supernatant was collected and analyzed using the Secrete-
405 Pair Dual Luminescence Assay Kit (cat # LF031) to measure luciferase activity following the
406 manufacturer's protocol. The fold induction was calculated after normalizing the values against
407 secreted alkaline phosphatase luminescence, used as an internal control.

408

409 **RNA isolation and quantitative real-time PCR.**

410 Total RNA isolation and qRT-PCR analysis was conducted in indicated PC cell lines as
411 described previously [18]. The qRT-PCR primers are listed in Table **S4**.

412

413 **Generation of CRISPR-Cas9 mediated inducible ECD Knockout (KO) cell lines.**

414 To generate inducible ECD KO cell lines, Lentiviral supernatants were generated as

415 mentioned above for Edit-R inducible Lentiviral hEF1a-Blast-Cas9 plasmid (cat # CAS11229) and
416 Edit-R lentiviral plasmids carrying guide RNAs against non-targeting control (NTC) (cat #
417 GSG11811), or human ECD gRNA1 (cat # GSGH11838-246505144, Seq-
418 TCCAAAGTCTCAACCCACAA) or gRNA2 (cat # GSGH11838-246505139, Seq-
419 CTTGGGTATACTTACCCTAT). All plasmids were procured from horizon discovery. Cells
420 were transduced first for cas-9 expression, then selected in medium containing 5 µg/ml blasticidin
421 for 5 days. Inducible Cas-9 expressing cells were then transduced with either NTC or gRNA1/2
422 lentiviral supernatants and selected in 5 µg/ml blasticidin + 1 µg/ml puromycin for additional 5
423 days.
424
425 **Transwell migration and invasion assays:**
426 Cell lines were subjected to serum deprivation (cultured in complete RPMI medium with
427 0.5 % FBS) for 24 h, trypsinized and seeded in transwell migration (Corning BioCoat 8.0 µm cat
428 # 354578) or invasion (BioCoat Matrigel 8.0 µm cat # 354480) chambers at 100,000 cells per well
429 in 0.5% FBS containing medium. After three hours of incubation at 37°C, complete RPMI medium
430 containing 10% FBS was added as a chemoattractant in the bottom chambers. After 24 h of
431 incubation, the cells on the top of filters were scrapped off and the migrated cells on the bottom of
432 filters were fixed in ice-cold methanol, stained with crystal violet, and rinsed in PBS. Cells in six
433 random fields per well were imaged at 100x magnification and quantified using the ImageJ
434 software. Experiments were repeated three times independently with triplicates each time.
435
436 **Anchorage-independent growth assays.**
437 20,000 vector-control or ECD-OE cells in complete RPMI medium containing 0.3%

438 agarose were seeded on top of a 0.6% bottom layer of agarose in 6-well plates, as described [5 6].
439 Cultures were fed every 2 days. Twenty-one days after cell seeding, the colonies were stained with
440 0.05% crystal violet in 25% methanol. Colonies were imaged under 10x magnification with phase
441 contrast microscope and counted using the image J software. Experiments were performed in
442 triplicates, and each experiment was repeated three times.

443

444 **Matrigel organoid cultures.**

445 2,000 vector-control or ECD-OE cells resuspended in the medium containing 4%
446 Matrigel were seeded per well on top of a base layer of 100% Matrigel in eight-well Nunc
447 chamber slides. The cells were allowed to form organoid colonies for 6 days and then imaged.
448 The ImageJ software was used for quantification with a size cut-off of 70 μm in diameter. All
449 experiments were performed in triplicate wells and repeated three times.

450

451 **Prostate cancer patient tissue microarrays and immunohistochemical analysis.**

452 The prostate cancer tissue specimens were obtained with informed consent from patients
453 who underwent radical prostatectomy at the Department of Urology, Institute for Pathology,
454 University Hospital "Carl-Gustav-Carus", University of Technology, Dresden between 1999 and
455 2005. Patient age ranged between 43 and 74 years (median 60 years). Preoperative PSA levels
456 ranged from 0.8 to 39 ng/ml (median 7.2). Clinical follow-up data was assessed annually.
457 The distribution of Gleason scores (GS) in the cohort was as follows: GS 2–6: 192 (34.5%), GS 7-
458 10: 364 (65.5%). Three hundred and eighty-six cases had organ-confined carcinomas (pT2); 170
459 cases showed extracapsular tumor extension (pT3). The surgical margins were clear (R0) in 396
460 cases; 157 cases had positive margins (R1). The median follow-up time of all cases was 60 months.

461 Tissue microarrays (TMAs) composed of 556 cases of paired normal/hyperplastic prostate and
462 prostate cancer (one core per case) were analyzed for ECD expression using an anti-ECD
463 monoclonal antibody [13]. 542 samples were classified as normal, 401 samples were hyperplastic,
464 and 258 samples were classified as high-grade PIN. We have followed data of 522 prostate cancer
465 patients (each patient was represented only once, so 556 tumors are from 566 different patients).
466 The intensity of staining was expressed as a semiquantitative scoring system: negative = 0, low =
467 1, moderate = 2 and High =3. Stratification into ECD-High vs ECD-Low expression status reflects
468 cases with staining intensity of 0 or 1 vs. 2 or 3, respectively. Kaplan-Meier survival analysis
469 compared 224 ECD-High (2-3) vs. 298 ECD-Low (< or = 1) cases. A pathologist evaluated all
470 slides. ECD expression (low vs. high), tumor grade (Gleason 1–6 vs. 7–10), pT-stage (pT1/2vs.
471 pT3/4), R-status (R0 vs. R1), age (<60 years vs. >60 years) and pre-operative PSA (low/<7.2 vs.
472 high/>7.2 ng/ml) were used in multivariate Cox regression analysis. The Charite approved the use
473 of PC tissue samples by the University Ethics Committee under the protocol 'Retrospective
474 analysis of tissue samples by immunohistochemistry and molecular biological techniques'
475 (EA1/06/2004) on 20 September 2004.
476
477 **ECD overexpression in prostate cancer cell lines.**
478 The ECD (GeneID: 11319) CDS in the mammalian expression vector pLenti-C-Myc-
479 DDK-P2A-Puro and empty Vector control plasmids were obtained from (Origene Biotech cat #
480 PS100092). Lentiviral supernatants were generated by transient co-transfection of Lenti-X 293T
481 cells with ECD expression vector and packaging plasmids psPAX2 (Addgene, cat # 12260) and
482 pMD2.G (Addgene cat # 12259) using X-treme GENE HP DNA transfection reagent (Roche cat
483 # 06366236001). Collected lentiviral supernatant was added to PC cells in the presence of

484 polybrene (8 µg/ml, Sigma # H9268). Post-infection, transduced cells were selected in 1 µg/ml
485 puromycin for 5 days, and ECD levels assessed by Western blotting using an anti-ECD monoclonal
486 antibody [13]. For siRNA KD, cells were transfected with 40 nM of control or gene-specific
487 siRNAs (AR siRNA, Santa Cruz, cat # SC29204) using the DharmaFECT 1 transfection reagent (cat
488 # T-2001-03, Dharmacon, Pittsburgh, PA).
489
490 **Cell proliferation assay.**
491 2,000 cells were plated per well in 96 well plates, with six replicates for each condition.
492 Medium was changed on alternate days. Cell proliferation was measured at the indicated times
493 using the Cell Titer- Glo® luminescent cell viability assay (Promega, cat # G7570) following the
494 manufacturer's protocol.
495
496 **Xenograft studies and IVIS imaging**.
497 All animal experiments were pre-approved by the UNMC Institutional Animal Care and
498 Use Committee (IACUC Protocol # 22-059-10-FC). To assess the effect of ECD OE on
499 tumorigenesis, $3x10^6$ vector control or ECD-OE LNCaP cells engineered with lentiviral
500 mCherry-luciferase in 0.1 ml 50% Matrigel (BD Biosciences) in cold PBS were injected
501 subcutaneously in 8-week-old athymic nude male mice (n=14) on both sides of dorsal flank. Tumor
502 growth was monitored twice a week using calipers and once a week by IVIS bioluminescence
503 imaging for up to 37 days. Tumor volume was calculated as length x width x depth/2 [23]. Mice
504 were euthanized when mice reached pre-determined humane endpoints or reached 2 cm^3 in
505 volume, as per the institutional IACUC guidelines. For IVIS imaging, mice received 200 µl D-
506 luciferin (15 mg/ml in PBS; Millipore Sigma #L9504) intraperitoneally 15 min before isoflurane

507 anesthesia and were placed dorsoventrally in the IVIS™ Imaging System (IVIS 2000). Images
508 were acquired using the IVIS Spectrum CT and analyzed using the Living Image 4.4 software
509 (PerkinElmer). The fold change in total Photon flux (p/s) over time was used to compare tumor
510 growth between the vector and ECD-OE cells groups.

511

512 **Immunohistochemistry of mice tumors.**

513 The mouse tumors harvested at necropsy were fixed in 10% neutral buffered formalin (cat
514 # 316- 155; PROTOCOL), paraffin-embedded and 5 mm sections deparaffinized in xylene and
515 rehydrated in descending alcohols followed by IHC staining of indicated antibodies as previously
516 described [23]. Periodic Acid Schiff's staining of tumor sections was conducted in tissue science
517 core facility of the University of Nebraska Medical Center.

518 **RNA sequencing, bioinformatics, and statistical analysis.**

519 Trizol-isolated total RNA from the core piece of the isolated tumors was analyzed on a
520 Bioanalyzer for quality and purity. RNA-seq libraries were prepared and subjected to 100 bp
521 paired-end sequencing on an Illumina NovaSeq 6000 system (UNMC Genomics Core). Analysis
522 of RNA-seq results was done using the nf-core RNA-seq pipeline version 3.9 [64], accessed via
523 Nextflow version 22.10.3 [65] and executed with Singularity [66] to ensure reproducibility and
524 portability. Paired-end sequencing reads were aligned to the human reference genome (GRCh38)
525 using the Spliced Transcripts Alignment to a Reference (STAR) software version 2.7.11a [67],
526 incorporating Ensemble gene annotations for accurate mapping. Quantification of transcript
527 abundance was performed using StringTie2 version 1.3.6 [68], with transcripts per million (TPM)
528 normalization to facilitate comparison across samples. Differential expression analysis between
529 vector and ECD-OE xenograft tumors was conducted using DESeq2 [69]. Differentially expressed

530 genes were identified using criteria of an adjusted p-value < 0.05 and a minimum twofold change
531 in expression. For functional interpretation of the differential expression results, we utilized the
532 Gene Set Enrichment Analysis (GSEA) software from the Broad Institute [70]. Enrichment plots
533 were generated to visualize the distribution of gene sets and to identify pathways significantly
534 associated with the observed transcriptional changes.

535

536 **RNA Immunoprecipitation (RIP) assay.**

537 RIP assays were performed using the EZ-Magna RIP Kit (Millipore, cat #17-701). Briefly,
538 cells were harvested and lysed using RIP lysis buffer with 1 freeze-thaw cycle. Cellular debris was
539 removed by centrifuging the cell lysates at 13K for 15 min. 1 mg aliquots of clarified lysate (BCA
540 method) were incubated overnight at 4°C with protein A Dynabeads bound to 2.5 µg of polyclonal
541 rabbit anti-ECD (Proteintech, cat # 10192-1-AP) or control IgG (Abcam cat #
542 ab172730) antibodies. Post incubation samples were subjected to five washes in the wash buffer.
543 The bound RNAs were retrieved and subjected to qRT-PCR analysis using gene specific primers.
544 10% of lysates served as input controls.

545

546 **Analysis of mRNA stability.**

547 cell lines were seeded in 6-well plates (200,000 cells per well). 24 h after plating, 5 µg/ml
548 actinomycin D (catalog # A1410; Sigma, St. Louis, MO) was added and total RNA isolated at the
549 indicated time points using the TRIzol method. cDNA was synthesized using iScript™ gDNA
550 Clear cDNA Synthesis Kit (Bio-Rad), as above, followed by qRT-PCR with the indicated gene
551 specific primers.

552

553 **Glucose Uptake-Glo assay:**

554 Cells were seeded at 25,000 cells per well in 96-well plates. 24 h later, the cells were
555 washed twice with PBS and cultured in glucose-free DMEM media (Thermo Scientific cat #
556 11966025) for 1 h (glucose starvation). Glucose uptake assay was then performed using the
557 Promega Glucose Uptake-Glo (J1341) assay kit according to the manufacturer's protocol. Parallel
558 CellTiter-Glo assays were used for normalization of cell numbers.

559

560 **Seahorse XF Glycolytic Rate Assay.**

561 The Oxygen Consumption Rate (OCR), Extracellular Acidification Rate (ECAR) and
562 Proton Efflux rate (PER) were measured using the Seahorse XFe Glycolytic rate assay Kit (Agilent
563 Technologies; cat #103344-100) according to the manufacturer's protocol. Briefly, 3.5×10^4 cells
564 were seeded per well in 96-well Seahorse XFe cell culture plates and incubated overnight. Cells
565 were washed and incubated with XF assay medium supplemented with 1 mM pyruvate (Sigma;
566 cat# S8636), 2 mM L-glutamine (Invitrogen; cat#25030081) and 10 mM glucose (Gibco;
567 cat#A24940-01) for 1 h at 37°C in a CO_2-free incubator. The OCR, ECAR and PER estimations
568 were performed as per the manufacturer's instructions. Basal OCR and ECAR were assessed in
569 response to rotenone/antimycin A (0.5 μM) and 2-deoxy-D-glucose (2-DG; 50 mM). ATP rate was
570 estimated in response to oligomycin (1.5 μM) and rotenone/antimycin A (0.5 μM). Basal
571 glycolysis was calculated from non-glycolytic acidification (background) ECAR/PER. Glycolytic
572 reserve (Compensatory) was calculated as the difference between glycolytic capacity and basal
573 glycolysis.

574

575 **Statistical analysis.**

576 Statistical analyses were done using the GraphPad Prism 11 software. Significance
577 between two groups was determined by the two-tailed Student's t test. Comparisons among three
578 or more groups were made using either one-way ANOVA or two-way ANOVA with post hoc
579 multiple comparisons test. A p-value of ≤0.05 was considered statistically significant. Survival
580 curves were analyzed using the Kaplan-Meier analysis with the log rank test. The results are
581 expressed as the mean ± SEM from three independent experiments, done in triplicates. The type
582 of statistical test used in individual experiments is indicated in figure legends.
583
584
585 **Acknowledgements:** This research was funded by Pilot grants from the Fred & Pamela Buffett
586 Cancer Center (HB & VB); Department of Defense grants W81XWH-17-1-0616 and W81XWH-
587 20-1-0058 to HB and W81XWH-20-1-0546, HT94252410337; and NIH grants R21CA241055
588 and R03CA253193 to VB; the NIH Pathway to Independence Award R00 GM1287671and the
589 NIH MIRA award R35 GM147467 (to M.J.R.); the Raphael Bonita Memorial Fund, and support
590 to UNMC core facilities from the NCI Cancer Center Support Grant (P30CA036727) awarded to
591 Fred & Pamela Buffett Cancer Center and from the Nebraska Research Initiative.
592 **Author Contributions:**
593 Conceptualization and design: M.R., A.R.R., B.B.K., T.E.R., F.O., S.M., M.J.R., G.K., K.D.,
594 B.C.M., H.B., and V.B.
595 manuscript writing; M.R., A.R.R., B.C.M., T.E.R., K.D., M.J.R., H.B., and V.B.
596 data analysis and interpretation. M.R., A.R.R., B.B.K., T.E.R., F.O., S.M., M.J.R., G.K., K.D.,
597 B.C.M., H.B., and V.B.
598 manuscript editing; M.J.R., B.C.M., H.B., and V.B.

599 bioinformatics analysis for the manuscript. M.R., T.E.R., M.J.R.,

600 All authors have read and approved the final version of the manuscript and agree with the order

601 of presentation of the authors.

602 **Competing Interests:**

603 Dr. H. Band and Dr. V. Band received funding from Nimbus Therapeutics for an unrelated

604 project. The remaining authors do not have any competing interest to declare.

605 **Data Availability Statement:**

606 The RNA-seq files generated in this study are available from the NCBI Gene Expression Omnibus

607 (GEO) under the accession number: GSE287898.

References:

608 1 Siegel RL, Miller KD, Wagle NS, Jemal A. Cancer statistics, 2023. *CA Cancer J Clin* 2023; 73:
609 17-48.
610
611 2 Huggins C, Hodges CV. Studies on prostatic cancer. I. The effect of castration, of estrogen and
612 androgen injection on serum phosphatases in metastatic carcinoma of the prostate. *CA Cancer J*
613 *Clin* 1972; 22: 232-240.
614
615 3 Rathkopf D, Scher HI. Androgen receptor antagonists in castration-resistant prostate cancer.
616 *Cancer J* 2013; 19: 43-49.
617
618 4 Watson PA, Arora VK, Sawyers CL. Emerging mechanisms of resistance to androgen receptor
619 inhibitors in prostate cancer. *Nat Rev Cancer* 2015; 15: 701-711.
620
621 5 Lokeshwar SD, Klaassen Z, Saad F. Treatment and trials in non-metastatic castration-resistant
622 prostate cancer. *Nat Rev Urol* 2021; 18: 433-442.
623
624 6 Ahmad F, Cherukuri MK, Choyke PL. Metabolic reprogramming in prostate cancer. *Br J Cancer*
625 2021; 125: 1185-1196.
626
627 7 Lasorsa F, di Meo NA, Rutigliano M, Ferro M, Terracciano D, Tataru OS *et al*. Emerging
628 Hallmarks of Metabolic Reprogramming in Prostate Cancer. *Int J Mol Sci* 2023; 24.
629
630 8 de Wet L, Williams A, Gillard M, Kregel S, Lamperis S, Gutgesell LC *et al*. SOX2 mediates
631 metabolic reprogramming of prostate cancer cells. *Oncogene* 2022; 41: 1190-1202.
632

633 9 Mishra R, Haldar S, Placencio V, Madhav A, Rohena-Rivera K, Agarwal P *et al*. Stromal
634 epigenetic alterations drive metabolic and neuroendocrine prostate cancer reprogramming. *J Clin*
635 *Invest* 2018; 128: 4472-4484.
636
637 10 Flavin R, Zadra G, Loda M. Metabolic alterations and targeted therapies in prostate cancer. *J*
638 *Pathol* 2011; 223: 283-294.
639
640 11 Beier AK, Puhr M, Stope MB, Thomas C, Erb HHH. Metabolic changes during prostate cancer
641 development and progression. *J Cancer Res Clin Oncol* 2023; 149: 2259-2270.
642
643 12 Gaziova I, Bonnette PC, Henrich VC, Jindra M. Cell-autonomous roles of the ecdysoneless gene
644 in Drosophila development and oogenesis. *Development* 2004; 131: 2715-2725.
645
646 13 Kim JH, Gurumurthy CB, Naramura M, Zhang Y, Dudley AT, Doglio L *et al*. Role of
647 mammalian Ecdysoneless in cell cycle regulation. *J Biol Chem* 2009; 284: 26402-26410.
648
649 14 Olou AA, Sarkar A, Bele A, Gurumurthy CB, Mir RA, Ammons SA *et al*. Mammalian ECD
650 Protein Is a Novel Negative Regulator of the PERK Arm of the Unfolded Protein Response. *Mol*
651 *Cell Biol* 2017; 37.
652
653 15 Kim JH, Gurumurthy CB, Band H, Band V. Biochemical characterization of human Ecdysoneless
654 reveals a role in transcriptional regulation. *Biol Chem* 2010; 391: 9-19.
655
656 16 Claudius AK, Romani P, Lamkemeyer T, Jindra M, Uhlirova M. Unexpected role of the steroid-
657 deficiency protein ecdysoneless in pre-mRNA splicing. *PLoS Genet* 2014; 10: e1004287.
658
659 17 Malinova A, Cvackova Z, Mateju D, Horejsi Z, Abeza C, Vandermoere F *et al*. Assembly of the
660 U5 snRNP component PRPF8 is controlled by the HSP90/R2TP chaperones. *J Cell Biol* 2017;
661 216: 1579-1596.
662
663 18 Saleem I, Mirza S, Sarkar A, Raza M, Mohapatra B, Mushtaq I *et al*. The Mammalian
664 Ecdysoneless Protein Interacts with RNA Helicase DDX39A To Regulate Nuclear mRNA
665 Export. *Mol Cell Biol* 2021; 41: e0010321.
666
667 19 Mirza S, Kalluchi A, Raza M, Saleem I, Mohapatra B, Pal D *et al*. Ecdysoneless Protein
668 Regulates Viral and Cellular mRNA Splicing to Promote Cervical Oncogenesis. *Mol Cancer Res*
669 2022; 20: 305-318.
670
671 20 Dey P, Rachagani S, Chakraborty S, Singh PK, Zhao X, Gurumurthy CB *et al*. Overexpression of
672 ecdysoneless in pancreatic cancer and its role in oncogenesis by regulating glycolysis. *Clin*
673 *Cancer Res* 2012; 18: 6188-6198.
674
675 21 Xu SH, Huang JZ, Xu ML, Yu G, Yin XF, Chen D *et al*. ACK1 promotes gastric cancer
676 epithelial-mesenchymal transition and metastasis through AKT-POU2F1-ECD signalling. *J*
677 *Pathol* 2015; 236: 175-185.
678
679 22 Xu SH, Huang JZ, Chen M, Zeng M, Zou FY, Chen D *et al*. Amplification of ACK1 promotes
680 gastric tumorigenesis via ECD-dependent p53 ubiquitination degradation. *Oncotarget* 2017; 8:
681 12705-12716.
682
683 23 Mohapatra BC, Mirza S, Bele A, Gurumurthy CB, Raza M, Saleem I *et al*. Ecdysoneless

684 Overexpression Drives Mammary Tumorigenesis through Upregulation of C-MYC and Glucose
685 Metabolism. *Mol Cancer Res* 2022; 20: 1391-1404.
686
687 24 Isaacs JT. Hormonally responsive versus unresponsive progression of prostatic cancer to
688 antiandrogen therapy as studied with the Dunning R-3327-AT and -G rat adenocarcinomas.
689 *Cancer Res* 1982; 42: 5010-5014.
690
691 25 Coutinho I, Day TK, Tilley WD, Selth LA. Androgen receptor signaling in castration-resistant
692 prostate cancer: a lesson in persistence. *Endocr Relat Cancer* 2016; 23: T179-T197.
693
694 26 Thalmann GN, Anezinis PE, Chang SM, Zhau HE, Kim EE, Hopwood VL *et al*. Androgen-
695 independent cancer progression and bone metastasis in the LNCaP model of human prostate
696 cancer. *Cancer Res* 1994; 54: 2577-2581.
697
698 27 Attardi BJ, Burgenson J, Hild SA, Reel JR. Steroid hormonal regulation of growth, prostate
699 specific antigen secretion, and transcription mediated by the mutated androgen receptor in
700 CWR22Rv1 human prostate carcinoma cells. *Mol Cell Endocrinol* 2004; 222: 121-132.
701
702 28 Korenchuk S, Lehr JE, L MC, Lee YG, Whitney S, Vessella R *et al*. VCaP, a cell-based model
703 system of human prostate cancer. *In Vivo* 2001; 15: 163-168.
704
705 29 Horoszewicz JS, Leong SS, Kawinski E, Karr JP, Rosenthal H, Chu TM *et al*. LNCaP model of
706 human prostatic carcinoma. *Cancer Res* 1983; 43: 1809-1818.
707
708 30 Decker KF, Zheng D, He Y, Bowman T, Edwards JR, Jia L. Persistent androgen receptor-
709 mediated transcription in castration-resistant prostate cancer under androgen-deprived conditions.
710 *Nucleic Acids Res* 2012; 40: 10765-10779.
711
712 31 Bisson I, Prowse DM. WNT signaling regulates self-renewal and differentiation of prostate
713 cancer cells with stem cell characteristics. *Cell Res* 2009; 19: 683-697.
714
715 32 Zhu YS, Cai LQ, You X, Cordero JJ, Huang Y, Imperato-McGinley J. Androgen-induced
716 prostate-specific antigen gene expression is mediated via dihydrotestosterone in LNCaP cells. *J*
717 *Androl* 2003; 24: 681-687.
718
719 33 Wang Q, Li W, Liu XS, Carroll JS, Janne OA, Keeton EK *et al*. A hierarchical network of
720 transcription factors governs androgen receptor-dependent prostate cancer growth. *Mol Cell*
721 2007; 27: 380-392.
722
723 34 Zambelli F, Pesole G, Pavesi G. Pscan: finding over-represented transcription factor binding site
724 motifs in sequences from co-regulated or co-expressed genes. *Nucleic Acids Res* 2009; 37: W247-
725 252.
726
727 35 Dreos R, Ambrosini G, Groux R, Cavin Perier R, Bucher P. The eukaryotic promoter database in
728 its 30th year: focus on non-vertebrate organisms. *Nucleic Acids Res* 2017; 45: D51-D55.
729
730 36 Bailey TL, Johnson J, Grant CE, Noble WS. The MEME Suite. *Nucleic Acids Res* 2015; 43:
731 W39-49.
732
733 37 Rajan P, Sudbery IM, Villasevil ME, Mui E, Fleming J, Davis M *et al*. Next-generation
734 sequencing of advanced prostate cancer treated with androgen-deprivation therapy. *Eur Urol*

735 2014; 66: 32-39.
736
737 38 Erb HHH, Oster MA, Gelbrich N, Cammann C, Thomas C, Mustea A *et al*. Enzalutamide-
738 induced Proteolytic Degradation of the Androgen Receptor in Prostate Cancer Cells Is Mediated
739 Only to a Limited Extent by the Proteasome System. *Anticancer Res* 2021; 41: 3271-3279.
740
741 39 Abazid A, Martin B, Choinowski A, McNeill RV, Brandenburg LO, Ziegler P *et al*. The
742 androgen receptor antagonist enzalutamide induces apoptosis, dysregulates the heat shock protein
743 system, and diminishes the androgen receptor and estrogen receptor beta1 expression in prostate
744 cancer cells. *J Cell Biochem* 2019; 120: 16711-16722.
745
746 40 Lee CH, Yu CC, Wang BY, Chang WW. Tumorsphere as an effective in vitro platform for
747 screening anti-cancer stem cell drugs. *Oncotarget* 2016; 7: 1215-1226.
748
749 41 Bredholt G, Mannelqvist M, Stefansson IM, Birkeland E, Bo TH, Oyan AM *et al*. Tumor necrosis
750 is an important hallmark of aggressive endometrial cancer and associates with hypoxia,
751 angiogenesis and inflammation responses. *Oncotarget* 2015; 6: 39676-39691.
752
753 42 Gerdes J, Li L, Schlueter C, Duchrow M, Wohlenberg C, Gerlach C *et al*. Immunobiochemical
754 and molecular biologic characterization of the cell proliferation-associated nuclear antigen that is
755 defined by monoclonal antibody Ki-67. *Am J Pathol* 1991; 138: 867-873.
756
757 43 Tabrizian N, Nouruzi S, Cui CJ, Kobelev M, Namekawa T, Lodhia I *et al*. ASCL1 is activated
758 downstream of the ROR2/CREB signaling pathway to support lineage plasticity in prostate
759 cancer. *Cell Rep* 2023; 42: 112937.
760
761 44 Smith BA, Sokolov A, Uzunangelov V, Baertsch R, Newton Y, Graim K *et al*. A basal stem cell
762 signature identifies aggressive prostate cancer phenotypes. *Proc Natl Acad Sci U S A* 2015; 112:
763 E6544-6552.
764
765 45 Agell L, Hernandez S, Nonell L, Lorenzo M, Puigdecanet E, de Muga S *et al*. A 12-gene
766 expression signature is associated with aggressive histological in prostate cancer: SEC14L1 and
767 TCEB1 genes are potential markers of progression. *Am J Pathol* 2012; 181: 1585-1594.
768
769 46 Islam R, Mishra J, Polavaram NS, Bhattacharya S, Hong Z, Bodas S *et al*. Neuropilin-2 axis in
770 regulating secretory phenotype of neuroendocrine-like prostate cancer cells and its implication in
771 therapy resistance. *Cell Rep* 2022; 40: 111097.
772
773 47 Raza M, Rajan AR, Kalluchi A, Saleem I, Kennedy BB, Bhakat KK *et al*. ECD functions as a
774 novel RNA-binding protein to regulate mRNA splicing. *bioRxiv* 2025: 2025.2001.2024.634785.
775
776 48 Erkelenz S, Stankovic D, Mundorf J, Bresser T, Claudius AK, Boehm V *et al*. Ecd promotes U5
777 snRNP maturation and Prp8 stability. *Nucleic Acids Res* 2021; 49: 1688-1707.
778
779 49 Warburg O, Wind F, Negelein E. The Metabolism of Tumors in the Body. *J Gen Physiol* 1927; 8:
780 519-530.
781
782 50 Xie H, Song J, Godfrey J, Riscal R, Skuli N, Nissim I *et al*. Glycogen metabolism is dispensable
783 for tumour progression in clear cell renal cell carcinoma. *Nat Metab* 2021; 3: 327-336.
784
785 51 Chen Y, Zhou Q, Hankey W, Fang X, Yuan F. Second generation androgen receptor antagonists

786 and challenges in prostate cancer treatment. *Cell Death Dis* 2022; 13: 632.
787
788 52 Zhao X, Mirza S, Alshareeda A, Zhang Y, Gurumurthy CB, Bele A *et al*. Overexpression of a
789 novel cell cycle regulator ecdysoneless in breast cancer: a marker of poor prognosis in
790 HER2/neu-overexpressing breast cancer patients. *Breast Cancer Res Treat* 2012; 134: 171-180.
791
792 53 Kulik M, Bothe M, Kibar G, Fuchs A, Schone S, Prekovic S *et al*. Androgen and glucocorticoid
793 receptor direct distinct transcriptional programs by receptor-specific and shared DNA binding
794 sites. *Nucleic Acids Res* 2021; 49: 3856-3875.
795
796 54 Hiltunen J, Helminen L, Paakinaho V. Glucocorticoid receptor action in prostate cancer: the role
797 of transcription factor crosstalk. *Front Endocrinol (Lausanne)* 2024; 15: 1437179.
798
799 55 Acosta AM, Al Rasheed MRH, Rauscher GH, Vormittag E, Mon KS, Sharif A *et al*. Tumor
800 necrosis in radical prostatectomies with high-grade prostate cancer is associated with multiple
801 poor prognostic features and a high prevalence of residual disease. *Hum Pathol* 2018; 75: 1-9.
802
803 56 Bele A, Mirza S, Zhang Y, Ahmad Mir R, Lin S, Kim JH *et al*. The cell cycle regulator
804 ecdysoneless cooperates with H-Ras to promote oncogenic transformation of human mammary
805 epithelial cells. *Cell Cycle* 2015; 14: 990-1000.
806
807 57 Ma S, Chen Y, Quan P, Zhang J, Han S, Wang G *et al*. NPAS2 promotes aerobic glycolysis and
808 tumor growth in prostate cancer through HIF-1A signaling. *BMC Cancer* 2023; 23: 280.
809
810 58 Zhou Y, Zeng F, Richards GO, Wang N. ENO2, a Glycolytic Enzyme, Contributes to Prostate
811 Cancer Metastasis: A Systematic Review of Literature. *Cancers (Basel)* 2024; 16.
812
813 59 Cui Y, Nadiminty N, Liu C, Lou W, Schwartz CT, Gao AC. Upregulation of glucose metabolism
814 by NF-kappaB2/p52 mediates enzalutamide resistance in castration-resistant prostate cancer cells.
815 *Endocr Relat Cancer* 2014; 21: 435-442.
816
817 60 Gillis JL, Hinneh JA, Ryan NK, Irani S, Moldovan M, Quek LE *et al*. A feedback loop between
818 the androgen receptor and 6-phosphogluconate dehydrogenase (6PGD) drives prostate cancer
819 growth. *Elife* 2021; 10.
820
821 61 Liu J, Chen G, Liu Z, Liu S, Cai Z, You P *et al*. Aberrant FGFR Tyrosine Kinase Signaling
822 Enhances the Warburg Effect by Reprogramming LDH Isoform Expression and Activity in
823 Prostate Cancer. *Cancer Res* 2018; 78: 4459-4470.
824
825 62 Yang B, Chen W, Tao T, Zhang J, Kong D, Hao J *et al*. UBE2N promotes cell viability and
826 glycolysis by promoting Axin1 ubiquitination in prostate cancer cells. *Biol Direct* 2024; 19: 35.
827
828 63 Chakraborty S, Bhat AM, Mushtaq I, Luan H, Kalluchi A, Mirza S *et al*. EHD1-dependent traffic
829 of IGF-1 receptor to the cell surface is essential for Ewing sarcoma tumorigenesis and metastasis.
830 *Commun Biol* 2023; 6: 758.
831
832 64 Ewels PA, Peltzer A, Fillinger S, Patel H, Alneberg J, Wilm A *et al*. The nf-core framework for
833 community-curated bioinformatics pipelines. *Nat Biotechnol* 2020; 38: 276-278.
834
835 65 Di Tommaso P, Chatzou M, Floden EW, Barja PP, Palumbo E, Notredame C. Nextflow enables
836 reproducible computational workflows. *Nat Biotechnol* 2017; 35: 316-319.

66 Kurtzer GM, Sochat V, Bauer MW. Singularity: Scientific containers for mobility of compute. *PLoS One* 2017; 12: e0177459.

67 Dobin A, Davis CA, Schlesinger F, Drenkow J, Zaleski C, Jha S *et al*. STAR: ultrafast universal RNA-seq aligner. *Bioinformatics* 2013; 29: 15-21.

68 Kovaka S, Zimin AV, Pertea GM, Razaghi R, Salzberg SL, Pertea M. Transcriptome assembly from long-read RNA-seq alignments with StringTie2. *Genome Biol* 2019; 20: 278.

69 Love MI, Huber W, Anders S. Moderated estimation of fold change and dispersion for RNA-seq data with DESeq2. *Genome Biol* 2014; 15: 550.

70 Subramanian A, Tamayo P, Mootha VK, Mukherjee S, Ebert BL, Gillette MA *et al*. Gene set enrichment analysis: a knowledge-based approach for interpreting genome-wide expression profiles. *Proc Natl Acad Sci U S A* 2005; 102: 15545-15550.

Fig. 1

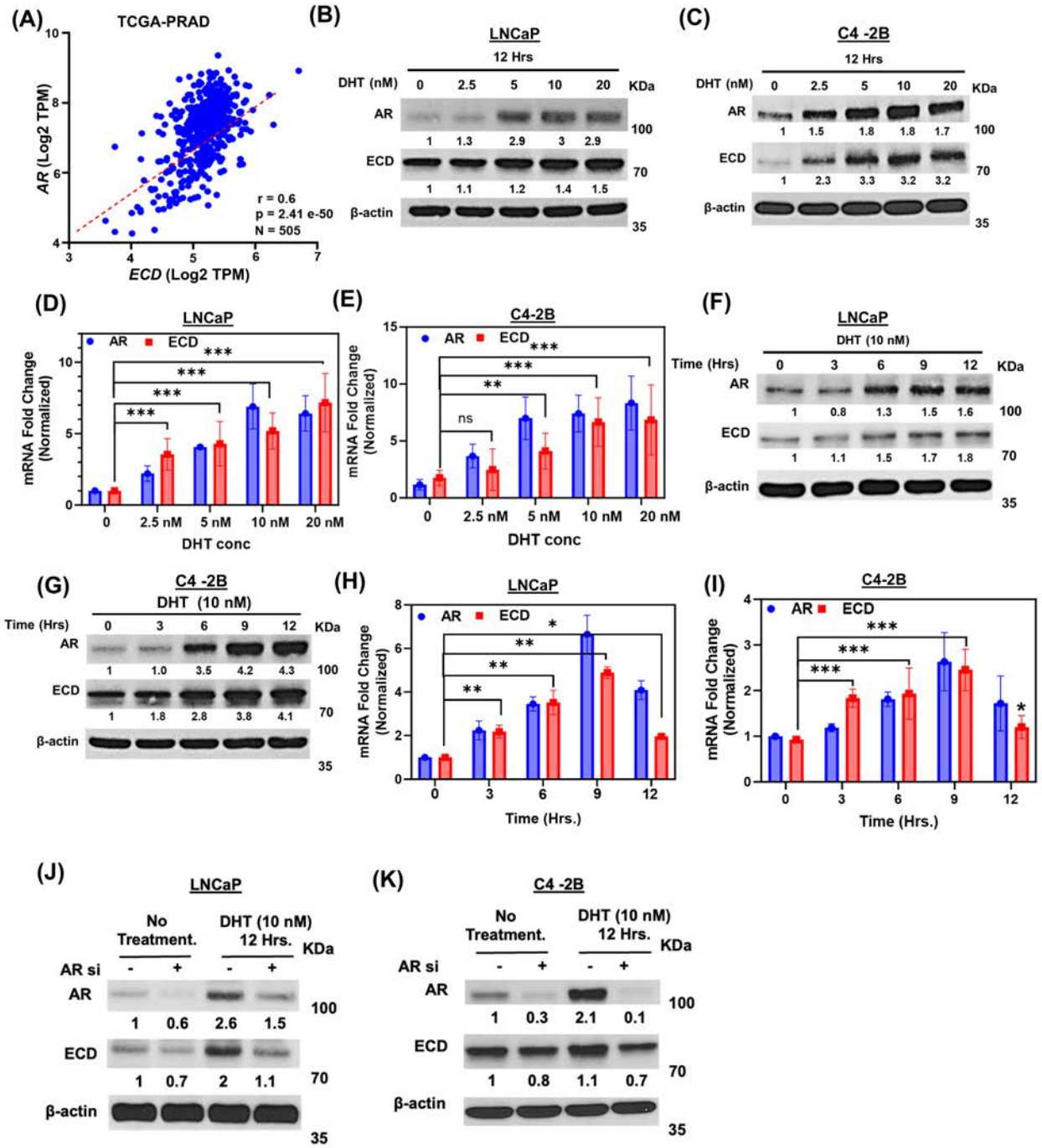
(A)
TCGA-PRAD
AR (Log2 TPM)
ECD (Log2 TPM)
r = 0.6
p = 2.41 e-50
N = 505
(B)
LNCaP
12 Hrs
DHT (nM) 0 2.5 5 10 20 KDa
AR 1 1.3 2.9 3 2.9 100
ECD 1 1.1 1.2 1.4 1.5 70
β-actin 35
(C)
C4 -2B
12 Hrs
DHT (nM) 0 2.5 5 10 20 KDa
AR 1 1.5 1.8 1.8 1.7 100
ECD 1 2.3 3.3 3.2 3.2 70
β-actin 35
(D)
LNCaP
AR ECD
mRNA Fold Change (Normalized)
DHT conc
0 2.5 nM 5 nM 10 nM 20 nM
(E)
C4-2B
AR ECD
mRNA Fold Change (Normalized)
ns
DHT conc
0 2.5 nM 5 nM 10 nM 20 nM
(F)
LNCaP
DHT (10 nM)
Time (Hrs) 0 3 6 9 12 KDa
AR 1 0.8 1.3 1.5 1.6 100
ECD 1 1.1 1.5 1.7 1.8 70
β-actin 35
(G)
C4 -2B
DHT (10 nM)
Time (Hrs) 0 3 6 9 12 KDa
AR 1 1.0 3.5 4.2 4.3 100
ECD 1 1.8 2.8 3.8 4.1 70
β-actin 35
(H)
LNCaP
AR ECD
mRNA Fold Change (Normalized)
Time (Hrs.)
(I)
C4-2B
AR ECD
mRNA Fold Change (Normalized)
Time (Hrs.)
(J)
LNCaP
No Treatment.
DHT (10 nM) 12 Hrs.
KDa
AR si - + - +
AR 1 0.6 2.6 1.5 100
ECD 1 0.7 2 1.1 70
β-actin 35
(K)
C4 -2B
No Treatment.
DHT (10 nM) 12 Hrs.
KDa
AR si - + - +
AR 1 0.3 2.1 0.1 100
ECD 1 0.8 1.1 0.7 70
β-actin 35

Fig. 1. Correlation of ECD and AR expression; AR regulates ECD expression. **(A)** Spearman's pairwise correlation plot illustrates a positive correction of AR and ECD mRNA in TCGA Prostate Adenocarcinoma Firehose dataset of cBioPortal online platform. Number of patients (N), correlation coefficient (r) and p-value are indicated on the plot. Pairwise correlation analysis was performed to calculate statistical significance. **(B & C)** Indicated PC cell lines were cultured in steroid free conditions for 72 hours. Cells were then treated with indicated concentrations of DHT for 12 hours and immunoblotted with anti-ECD or anti-AR antibodies. β- actin was used as a loading control. **(D & E)** qRT-PCR was performed in the same samples; RNA was isolated by standard TRIzol phenol chloroform method. 18s rRNA was used for normalization. **(F-I)** Similar protocols as mentioned above were used to perform a time response with DHT. Western blotting **(F & G)** and qRT-PCR **(H & I)** were performed on cell lysates, as above. **(J & K)** Indicated PC cell lines transfected with control siRNA or AR siRNA and cultured for 72 hours. Cells were then treated with indicated concentrations of DHT for 12 hours and then lysates were western blotted with anti-ECD or anti-AR antibodies. β- actin was used as a loading control in all blots. Numbers below the blots show the quantification of band intensities after normalizing with their respective loading control, β- actin in comparison with control samples using ImageJ software. Bar graphs represent mean ± SEM from three independent experiments, each done in triplicates. Student t-test was used to calculate statistical significance *** $p < 0.001$, ** $p < 0.01$, * $p < 0.05$, ns $p > 0.05$.

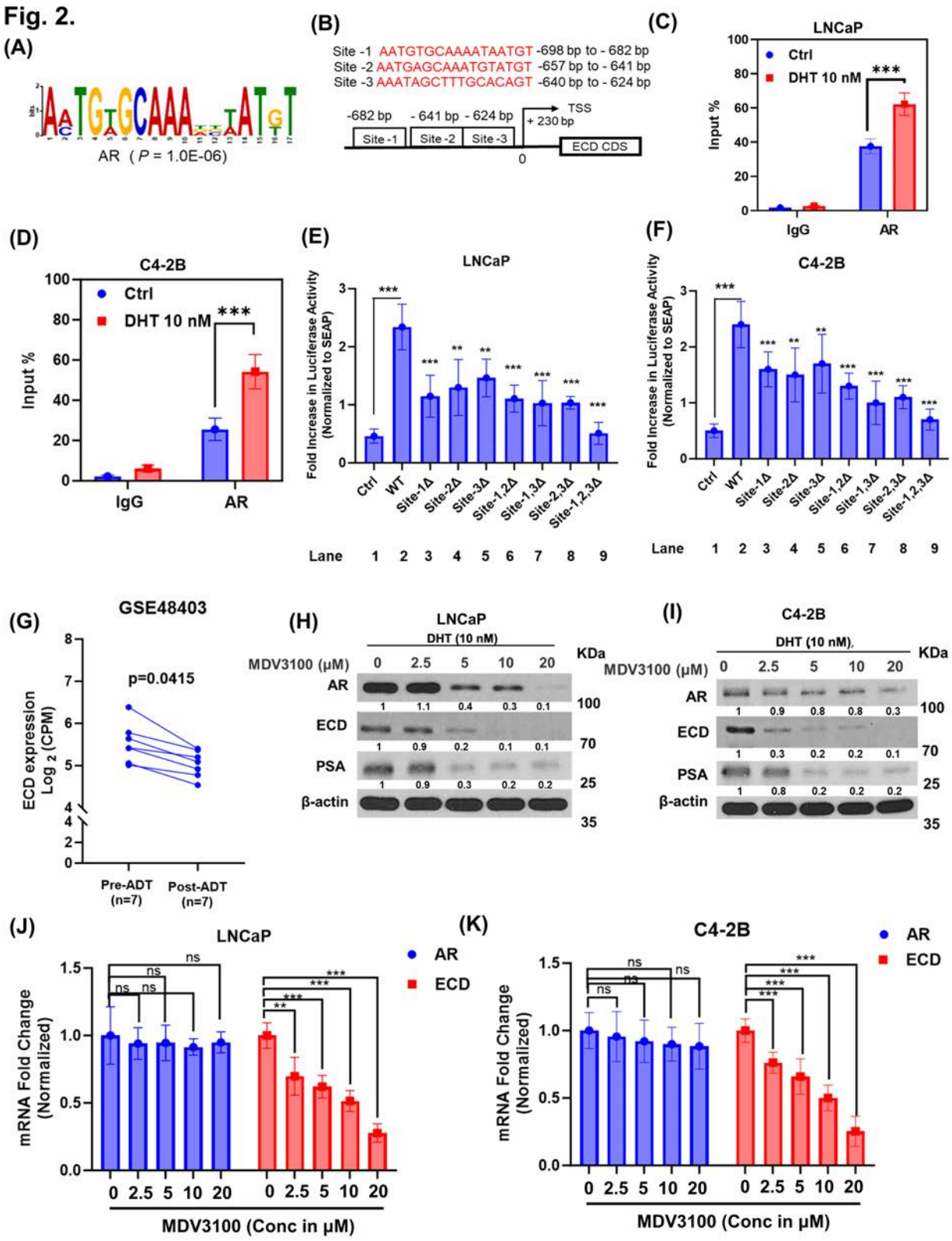
Fig. 2.
(A)
AR (P = 1.0E-06)
(B)
Site -1 AATGTGCAAAATAATGT -698 bp to - 682 bp
Site -2 AATGAGCAAATGTATGT -657 bp to - 641 bp
Site -3 AAATAGCTTTGCACAGT -640 bp to - 624 bp
-682 bp
- 641 bp - 624 bp
TSS
+ 230 bp
Site -1
Site -2
Site -3
ECD CDS
0
(C)
LNCaP
Ctrl
DHT 10 nM
***
Input %
IgG
AR
(D)
C4-2B
Ctrl
DHT 10 nM
***
Input %
IgG
AR
(E)
LNCaP
Fold Increase in Luciferase Activity (Normalized to SEAP)
Ctrl
WT
Site-1Δ
Site-2Δ
Site-3Δ
Site-1,2Δ
Site-1,3Δ
Site-2,3Δ
Site-1,2,3Δ
Lane 1 2 3 4 5 6 7 8 9
(F)
C4-2B
Fold Increase in Luciferase Activity (Normalized to SEAP)
Ctrl
WT
Site-1Δ
Site-2Δ
Site-3Δ
Site-1,2Δ
Site-1,3Δ
Site-2,3Δ
Site-1,2,3Δ
Lane 1 2 3 4 5 6 7 8 9
(G)
GSE48403
p=0.0415
ECD expression Log 2 (CPM)
Pre-ADT (n=7)
Post-ADT (n=7)
(H)
LNCaP
DHT (10 nM)
MDV3100 (μM) 0 2.5 5 10 20
KDa
AR
ECD
PSA
β-actin
100
70
25
35
(I)
C4-2B
DHT (10 nM),
MDV3100 (μM) 0 2.5 5 10 20
KDa
AR
ECD
PSA
β-actin
100
70
25
35
(J)
LNCaP
AR
ECD
mRNA Fold Change (Normalized)
MDV3100 (Conc in μM)
(K)
C4-2B
AR
ECD
mRNA Fold Change (Normalized)
MDV3100 (Conc in μM)

Fig. 2. Androgen treatment increased AR occupancy on ECD promoter and Enzalutamide treatment decreases ECD expression. (A & B) AR binding site**;** Top three predicted AR binding sites on the ECD promotor. **(C & D)** Chromatin immunoprecipitation (ChIP) analysis**.** Indicated cells were cultured in steroid-free conditions for 3 days, followed by dihydrotestosterone (DHT) treatment for 3 hours. Cells were cross-linked with formaldehyde and chromatin was immunoprecipitated with antibody against AR. IgG, used as a non-binding Control. Immunoprecipitated DNA was quantified with qPCR for specific binding sites at ECD promoter using primers encompassing all three sites -712 to -565 from transcription start site. Student t- test was performed to calculate statistical significance *** $p < 0.001$. **(E & F)** DHT increases ECD promoter activity. ECD promoter spanning approx. 1500 bp was cloned upstream of secreted Gaussia Luciferase, Secreted Alkaline phosphatase (SEAP) was used as an internal control. Cells expressing WT promoter or various AR binding sites deleted mutants were treated with 100 nM DHT for 3 hours. Supernatant was collected, and Luminescence was measured using Secrete-Pair Dual Luminescence Assay Kit. Data represents three independent experiments, each done in triplicates. *Student t- test* was performed to calculate statistical significance *** $p < 0.001$, ** $p < 0.01$. **(G)** Box plot depicting ECD mRNA expression in prostate tumors pre- and post-androgen deprivation therapy 7 samples in each case (GSE48403). A Wilcoxon matched-pairs signed-rank test was used to compare expressions in the groups. **(H & I**) Indicated PC cell lines were cultured in steroid-free medium for 72 hours, cells were then treated with 10 nM DHT, followed by treatment with indicated concentration of MDV3100 for another 48 hours. Lysates were collected and western blotted with indicated antibodies. β-actin was used as a loading control. **(J & K)** qRT-PCR was performed in the same samples where the RNA was isolated by standard TRIzol phenol

chloroform method. 18s rRNA was used for normalization. Bar graphs represent fold change in AR and ECD mRNA in LNCaP **(J)** and C4-2B cells **(K)** respect to vehicle treatment. Data represent mean ± SEM from three independent experiments, each done in triplicates. *Student t-test* was performed to calculate statistical significance *** $p < 0.001$, ** $p < 0.01$**.**

Fig. 3

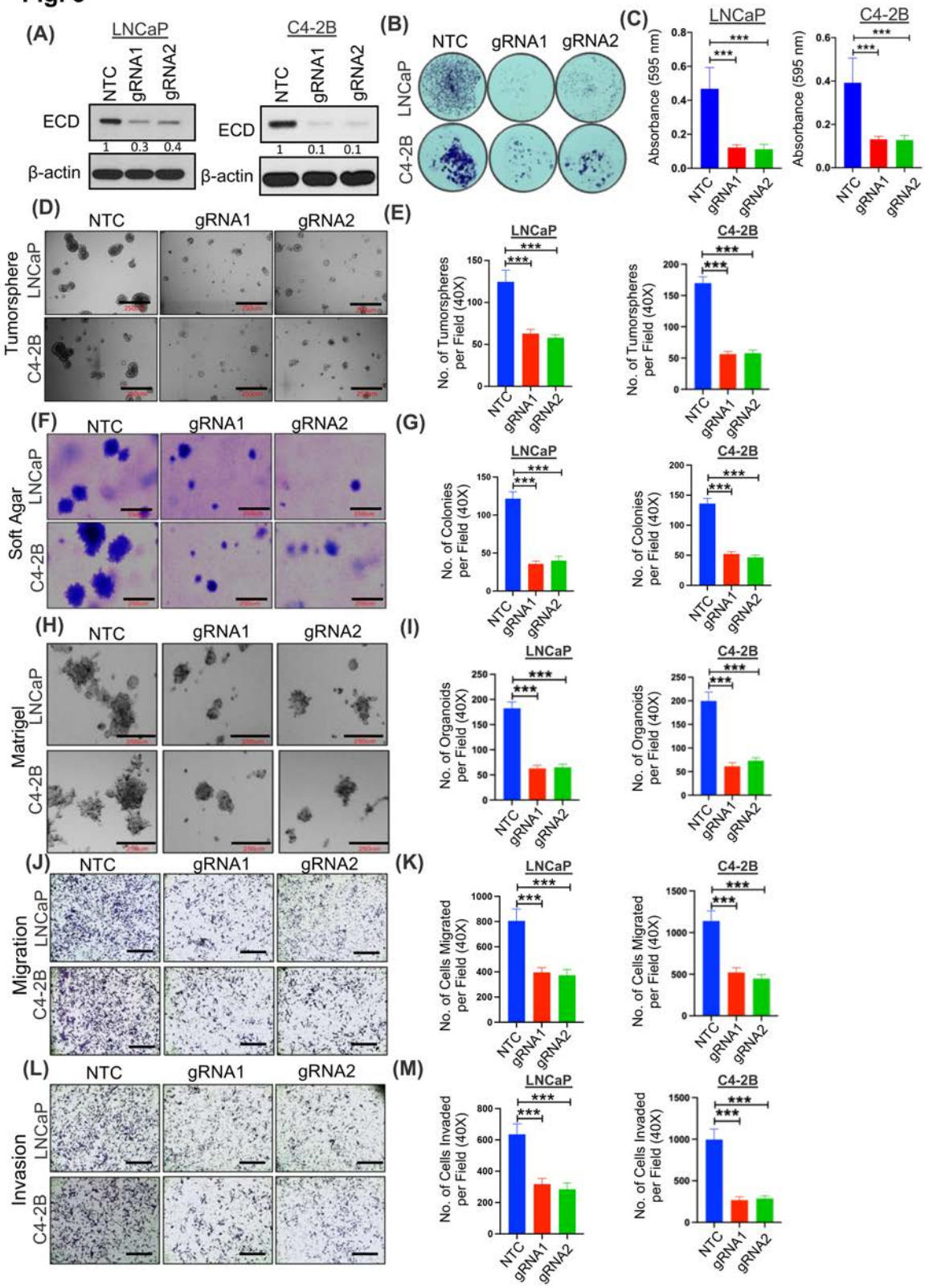
(A)
LNCaP
C4-2B
NTC
gRNA1
gRNA2
ECD
β-actin
1 0.3 0.4
1 0.1 0.1
(B)
NTC
gRNA1
gRNA2
LNCaP
C4-2B
(C)
LNCaP
C4-2B
Absorbance (595 nm)
***
(D)
Tumorsphere
(E)
No. of Tumorspheres per Field (40X)
(F)
Soft Agar
(G)
No. of Colonies per Field (40X)
(H)
Matrigel
(I)
No. of Organoids per Field (40X)
(J)
Migration
(K)
No. of Cells Migrated per Field (40X)
(L)
Invasion
(M)
No. of Cells Invaded per Field (40X)

Fig. 3. Depletion of ECD induces proliferation block and diminishes oncogenic traits in prostate cancer cells. LNCaP and C4-2B cells expressing doxycycline (Dox) regulated Cas9 and guide RNAs targeting either ECD (gRNA1 & 2) or non-targeting control (NTC) were cultured in the presence of Dox (1 μg/ml) for 96 hours to deplete ECD. **(A)** Western blot analysis. Numbers below the blots show the quantification of band intensities after normalizing with their respective loading control, β- actin in comparison with NTC using ImageJ software. Representative images and histograms depicting 2D (two dimensional) colony **(B & C),** tumorsphere **(D & E**), soft agar colony **(F & G),** Matrigel organoid formation **(H & I),** migration **(J & K)** and invasion **(L & M),** of control and ECD depleted PC cells lines. The representative images of tumorspheres, soft agar colonies and Matrigel organoids are 200x magnification, scale bar, 250 μm. Migration and invasion images are 40x magnification, scale bar, 1000 μm. The Bar graphs represent mean values ± SEM of three experiments done in triplicates from 40x magnification images. *Student t-test* was used to calculate statistical significance *** $p < 0.001$, ** $p < 0.01$.

Fig. 4

(A)

ECD_Tumor_Score_Cytoplasm

		Frequency	Percent	Valid Percent	Cumulative Percent
Valid	0	14	2.2	2.5	2.5
	1	301	47.0	54.1	56.7
	2	204	31.9	36.7	93.3
	3	37	5.8	6.7	100.0
	Total	556	86.9	100.0	
Missing	System	84	13.1		
Total		640	100.0		

(B)

Hyperplastic prostate tissue

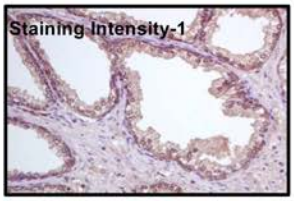

(C)

Prostate cancer

Low ECD expression

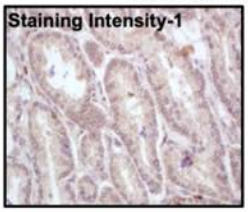

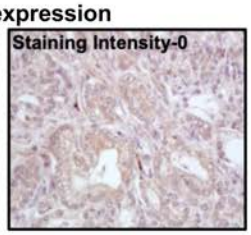

High ECD expression

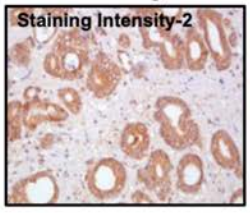

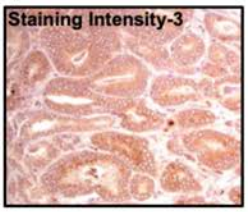

(D)

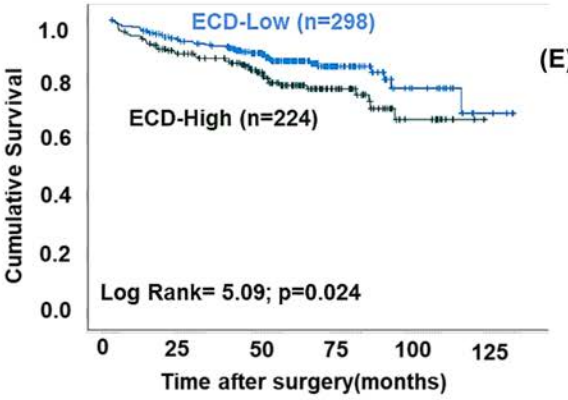

(E)

Case processing Summary

			Censored	
ECD_Tm cytoplasm 0,1v2,3	Total N	N of Events	N	Percent
0.00	298	42	256	85.9
1.00	224	47	177	79.0
Overall	522	89	433	83.0

(F)

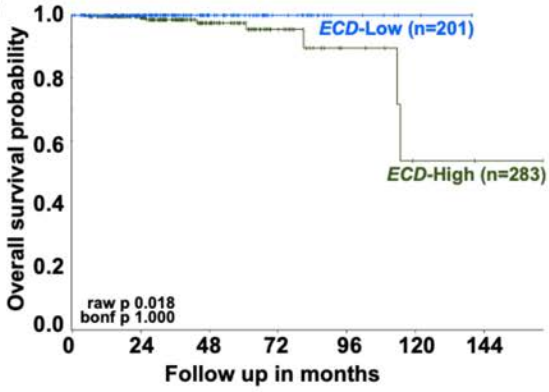

Fig. 4. Higher expression of ECD protein and mRNA in prostate cancer tissues correlate with short patient survival. (A) Frequency and percentage of patient TMA samples assigned to each staining intensity. **(B & C)** Representative IHC analysis of ECD expression in hyperplastic prostate tissue **(B),** and low-ECD (staining intensity 0, 1) and high-ECD expression (staining intensity 2, 3) in prostate cancer tissues **(C)** at magnification 200x. **(D)** Kaplan-Meier cumulative survival curve after surgery with patient tumors expressing low (staining intensities 0 or 1) or high ECD protein levels (staining intensities 2 or 3). P-values were calculated with a log-rank test. **(E)** Case processing summary with number and percent of events used for the overall survival analysis in Panel D is enlisted. N= number of patients, N of events= number of patients where outcome was known and censored means where the patients' outcome was unknown **(F)** Kaplan-Meier plot for survival curve of prostate cancer patients shows short survival in patients with tumors expressing high *ECD* mRNA (n=283) in comparison to low *ECD* mRNA (n=201). P-value is indicated in the KM plot. Mixed prostate adenocarcinoma (2022-v32) cohort (n=484) of The Cancer Genome Atlas (TCGA) dataset was used to stratify *ECD* mRNA expression as high (> 31.49 transcripts per million (TPM) and low (< 31.49 TPM). Analysis was performed using R2 Genomics platform.

Fig. 5.

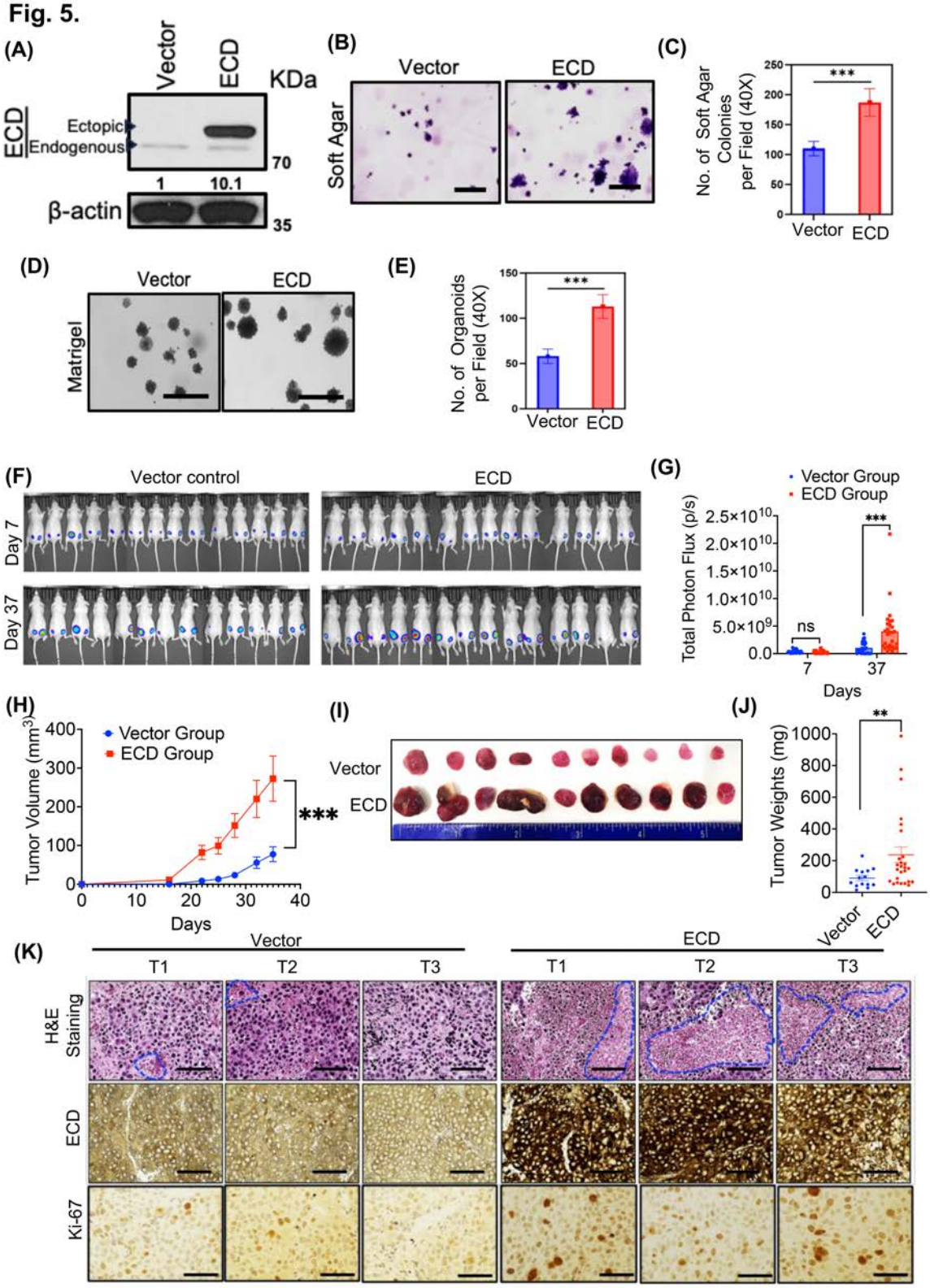
(A)
Vector
ECD
KDa
ECD
Ectopic
Endogenous
70
1
10.1
β-actin
35
(B)
Vector
ECD
Soft Agar
(C)
No. of Soft Agar Colonies per Field (40X)
***
Vector
ECD
(D)
Vector
ECD
Matrigel
(E)
No. of Organoids per Field (40X)
***
Vector
ECD
(F)
Vector control
ECD
Day 7
Day 37
(G)
Vector Group
ECD Group
Total Photon Flux (p/s)
ns
***
7
37
Days
(H)
Vector Group
ECD Group
Tumor Volume (mm3)
***
Days
(I)
Vector
ECD
(J)
Tumor Weights (mg)
**
Vector
ECD
(K)
Vector
ECD
T1
T2
T3
H&E Staining
ECD
Ki-67

Fig. 5. ECD overexpression in LNCaP cells exhibit enhanced *in vitro* oncogenic traits and *in vivo* tumorigenesis. (A) Western blot depicts ECD overexpression; densitometry in respect to vector cells after normalizing with β-actin, shown below. **(B)** Representative images in 100x magnification (scale bar, 400 μm) show soft agar colony formation abilities of cells. **(C)** Bars depict the quantitation of soft agar colonies per field at 40x magnification. **(D)** Representative images in 100x magnification (scale bar, 400 μm) depict 3D colony formation abilities in Matrigel. **(E)** Bar graphs show the quantitation of 3D colonies per field at 40x magnification. Data represents three independent experiments, each done in triplicates. ***$p < 0.001$, Student t-test was used to calculate statistical significance in (C) and (E)**. (F)** mCherry-luciferase expressing LNCaP-vector and ECD-OE cells were injected subcutaneously into nude mice (14/group) in both sides. Primary tumor growth was monitored by bioluminescence imaging at the indicated time on day 7 and day 37. **(G)** Bioluminescence signals of tumors over time are shown as change in photon flux over time. Data are mean ± SEM, n=14 (two sided tumors); Unpaired t-test; ***$p < 0.001$. **(H)** Tumor growth is followed over days with vernier caliper and fold change in tumor volume is plotted. Data are mean ± SEM, n=14; Two-way ANOVA (mixed model); ***$p < 0.001$. **(I)** Ten representative harvested tumors are displayed in each group. **(J)** Scattered plot represents the weights of harvested tumors. Data are mean ± SEM, n=14; unpaired t-test; **$p < 0.01$. **(K)** H&E and IHC analysis with ECD and Ki-67. Representative images from three independent tumors (T1, T2 and T3) from both groups, in 400x magnification (scale bar, 200 μm).

Fig. 6

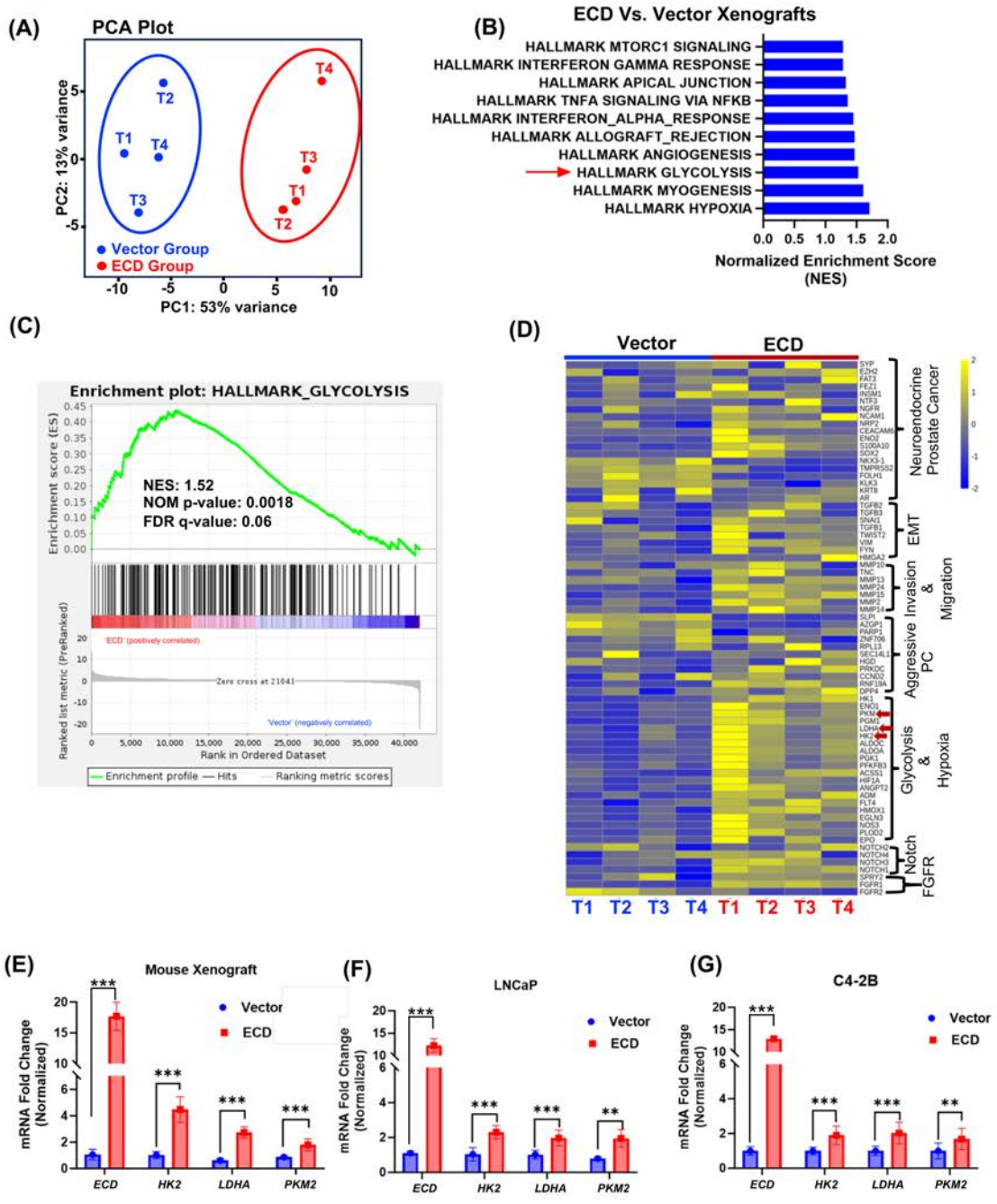
(A)
PCA Plot
PC2: 13% variance
PC1: 53% variance
T1
T2
T3
T4
Vector Group
ECD Group
(B)
ECD Vs. Vector Xenografts
HALLMARK MTORC1 SIGNALING
HALLMARK INTERFERON GAMMA RESPONSE
HALLMARK APICAL JUNCTION
HALLMARK TNFA SIGNALING VIA NFKB
HALLMARK INTERFERON_ALPHA_RESPONSE
HALLMARK ALLOGRAFT_REJECTION
HALLMARK ANGIOGENESIS
HALLMARK GLYCOLYSIS
HALLMARK MYOGENESIS
HALLMARK HYPOXIA
Normalized Enrichment Score (NES)
(C)
Enrichment plot: HALLMARK_GLYCOLYSIS
NES: 1.52
NOM p-value: 0.0018
FDR q-value: 0.06
Enrichment score (ES)
Ranked list metric (PreRanked)
Rank in Ordered Dataset
Enrichment profile
Hits
Ranking metric scores
(D)
Vector
ECD
Neuroendocrine Prostate Cancer
EMT
Invasion & Migration
Aggressive PC
Glycolysis & Hypoxia
Notch
FGFR
T1 T2 T3 T4 T1 T2 T3 T4
(E)
Mouse Xenograft
mRNA Fold Change (Normalized)
Vector
ECD
ECD
HK2
LDHA
PKM2
(F)
LNCaP
(G)
C4-2B

Fig. 6. ECD regulates mRNA expression of glycolytic and neuro endocrine signature genes. **(A)** Principal component analysis (PCA) analysis of RNA-seq data from LNCaP-vector expressing and LNCaP-ECD-OE xenograft tumors shows distinct clustering of datasets. **(B)** Bar plot displays enriched hallmark GSEA (Gene set enrichment analysis) gene sets. X-axis represents normalized enrichment scores (NES) of the signaling pathways with significant nominal p-values (NOM p-val) and <25% false discover rate q-values (FDR q-val). Red arrow indicates glycolysis (followed further in this study). **(C)** Enrichment plot of glycolysis in ECD-OE xenograft tumors compared to vector expressing xenograft tumors. NES, NOM p-val and FDR q-val. are indicated on the plot. **(D)** Heatmap of key glycolytic genes and indicated signature genes of PC oncogenic pathways is presented. Yellow represents upregulated and blue as downregulated genes. Major glycolytic genes are marked as red arrows. **(E-G)** qRT-PCR confirms the overexpression of *ECD* in xenograft tumors and prostate cancer cell lines. 18s rRNA was used for normalization. qRT-PCR analyses of indicated glycolytic genes. mRNA quantitation data represents mean ± SEM with two-tailed unpaired *t* test. n = 3; **, $p < 0.01$; ***, $p < 0.001$.

Fig. 7.

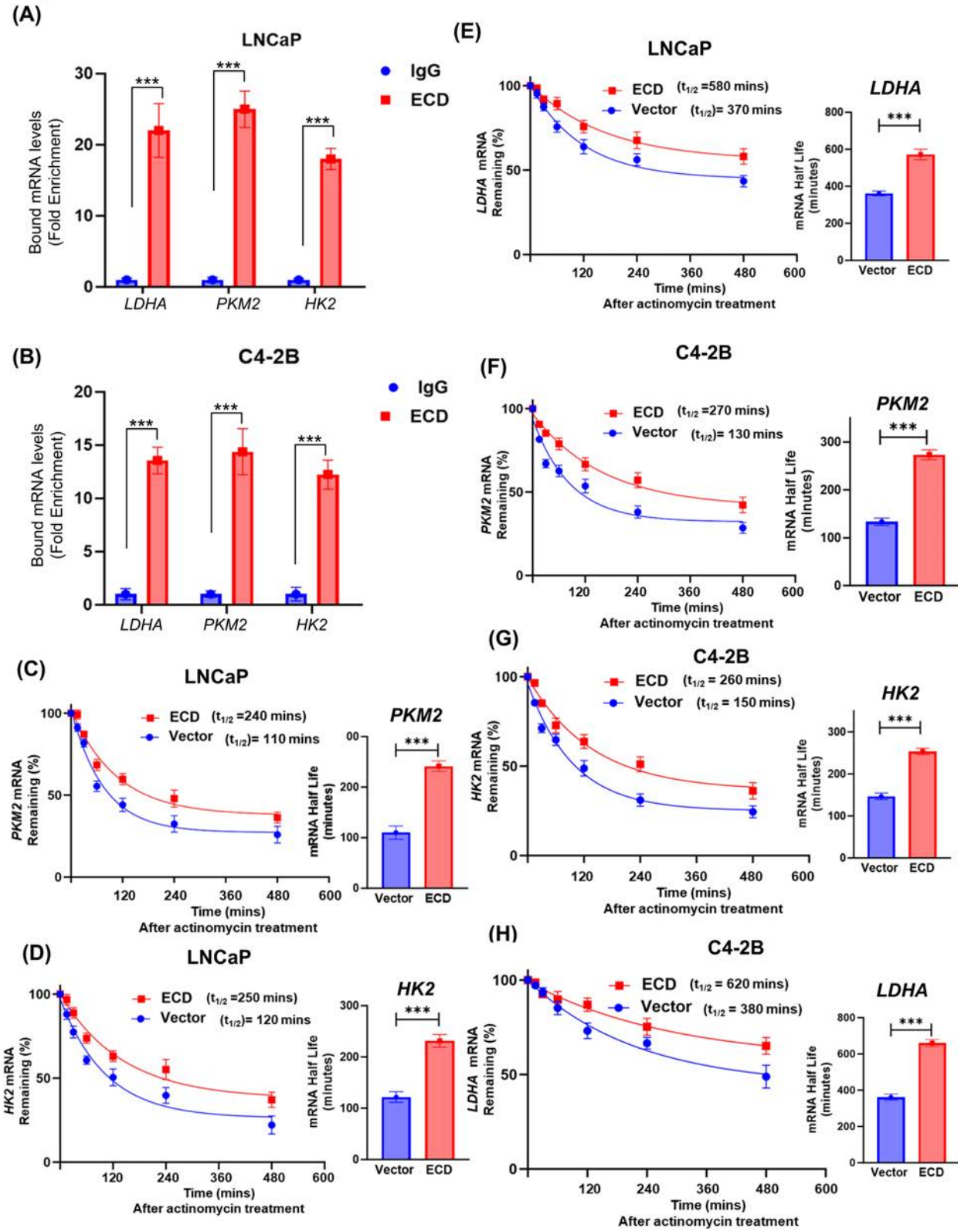
(A)
LNCaP
IgG
ECD
Bound mRNA levels (Fold Enrichment)
LDHA
PKM2
HK2
(B)
C4-2B
(C)
LNCaP
ECD (t1/2 =240 mins)
Vector (t1/2)= 110 mins
PKM2 mRNA Remaining (%)
Time (mins)
After actinomycin treatment
PKM2
mRNA Half Life (minutes)
Vector
ECD
(D)
LNCaP
ECD (t1/2 =250 mins)
Vector (t1/2)= 120 mins
HK2 mRNA Remaining (%)
HK2
(E)
LNCaP
ECD (t1/2 =580 mins)
Vector (t1/2)= 370 mins
LDHA mRNA Remaining (%)
LDHA
(F)
C4-2B
ECD (t1/2 =270 mins)
Vector (t1/2)= 130 mins
PKM2 mRNA Remaining (%)
PKM2
(G)
C4-2B
ECD (t1/2 = 260 mins)
Vector (t1/2 = 150 mins)
HK2 mRNA Remaining (%)
HK2
(H)
C4-2B
ECD (t1/2 = 620 mins)
Vector (t1/2 = 380 mins)
LDHA mRNA Remaining (%)
LDHA

Fig.7. ECD is associated with mRNAs of glycolytic enzymes and regulates their stability. (A & B). Indicated PC cells were subjected to RNA immunoprecipitation using IgG or anti-ECD antibodies and processed as per instructions in Magna RNA RIP kit. Co-precipitated RNAs were purified and the indicated target RNAs were detected by qRT-PCR using gene specific primers. Graph display mean fold enrichment in each respective gene, as compared to IgG control. **(C-H)** mRNA stabilities of various glycolytic enzymes after actinomycin D (5 µg/mL) treatment for indicated time points in vector or ECD expressing PC cells. Trend lines were created by measuring relative abundance of each transcript with respect to the 0-minute time point for vector and ECD-OE LNCaP and C4-2B cells and are expressed as percentage of mRNA remaining. Transcript abundance was measured by qRT-PCR using 18S rRNA as a housekeeping gene. Half-life ($t_{1/2}$) for indicated mRNAs are displayed for vector and ECD-OE cells. Bar graphs display mean fold enrichment in each respective gene, as compared to IgG control. Quantitation data represents mean ± SEM with two-tailed unpaired *t* test. n = 3; ***, $p < 0.001$.

Fig. 8.

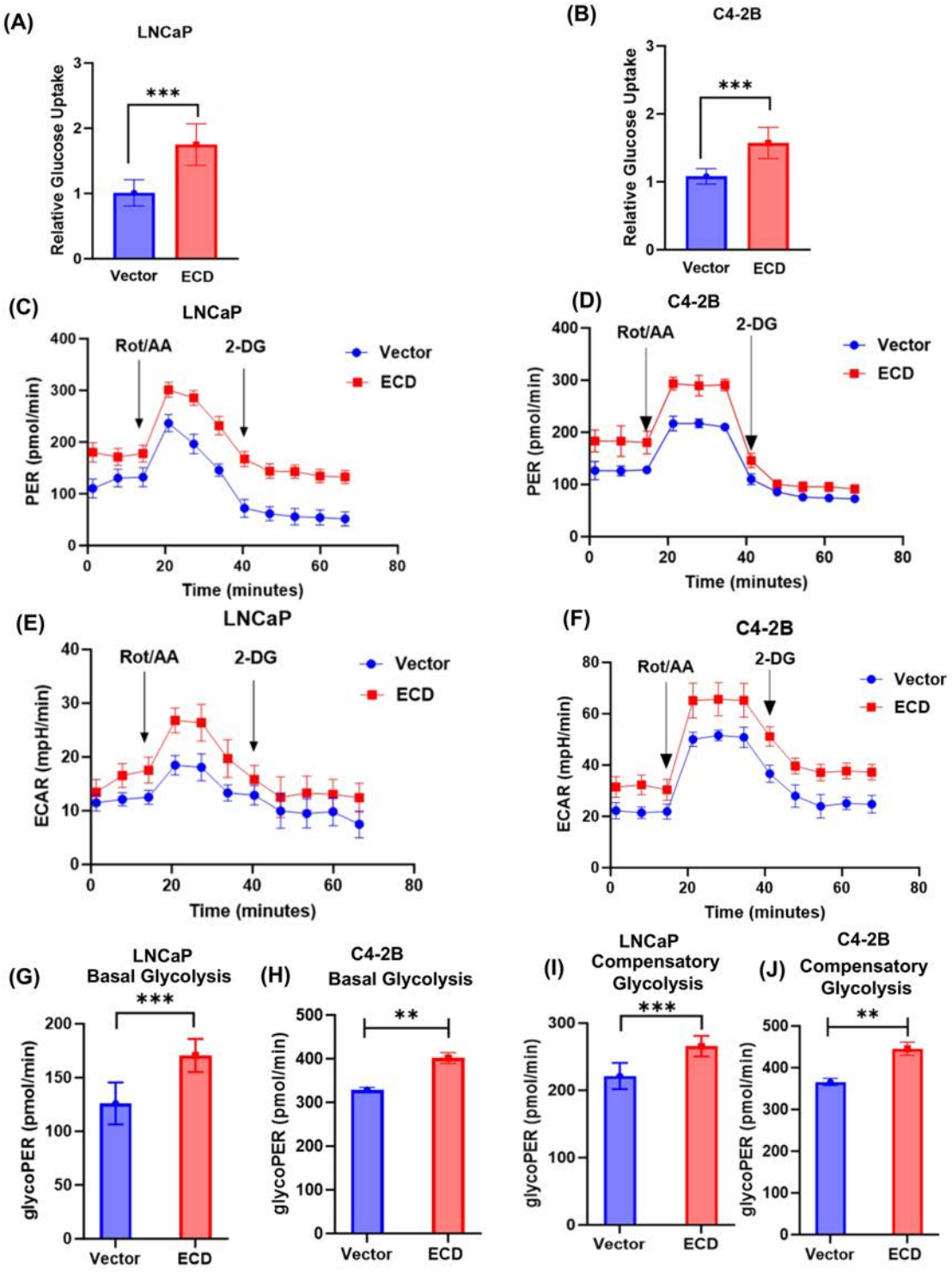
(A)
LNCaP
Relative Glucose Uptake
***
Vector
ECD
(B)
C4-2B
Relative Glucose Uptake
***
Vector
ECD
(C)
LNCaP
Rot/AA
2-DG
Vector
ECD
PER (pmol/min)
Time (minutes)
(D)
C4-2B
Rot/AA
2-DG
Vector
ECD
PER (pmol/min)
Time (minutes)
(E)
LNCaP
Rot/AA
2-DG
Vector
ECD
ECAR (mpH/min)
Time (minutes)
(F)
C4-2B
Rot/AA
2-DG
Vector
ECD
ECAR (mpH/min)
Time (minutes)
(G)
LNCaP
Basal Glycolysis
***
glycoPER (pmol/min)
Vector
ECD
(H)
C4-2B
Basal Glycolysis
**
glycoPER (pmol/min)
Vector
ECD
(I)
LNCaP
Compensatory
Glycolysis
***
glycoPER (pmol/min)
Vector
ECD
(J)
C4-2B
Compensatory
Glycolysis
**
glycoPER (pmol/min)
Vector
ECD

Fig. 8. ECD overexpression increases glucose uptake and glycolytic rate. Glucose uptake in LNCaP **(A)** and C4-2B **(B)** PC cell lines. The values were normalized with respective to cell counts and depicted as compared with vector control. Quantification of results from three biological experiments, each with six technical replicates is shown as a bar graph. Data represents mean ± SEM and two-tailed unpaired Student's t-test (*$p < 0.05$, **$p < 0.01$, ***$p < 0.001$). **(C-J)** Sea horse glycolytic rate was assessed in vector and ECD-OE LNCaP **(C)** and C4-2B **(E)** cells. Cells were seeded in 96-well plates and exposed to Rot/AA (rotenone and antimycin cocktail) and 2-DG to measure proton efflux rate **(PER, C & D)** and extracellular acidification rate **(ECAR, E & F)**. One representative PER and ECAR plots from three independent experiments are displayed (**C-F**). Basal glycolysis **(G & H)** and compensatory glycolysis **(I & J)** rates are presented as bar graphs, glycoPER in pmol/min calculated from subtracting ECAR (extra cellular acidification rate) from PER (proton efflux rates) (**G-J**). Quantitation data represents mean ± SEM with two-tailed unpaired *t* test. $n = 3$; **, $p < 0.01$; ***, $p < 0.001$.

Table S1

Multivariate Cox's regression analysis of prostate cancer patient tumors with inclusion of cytoplasmic ECD expression
RR: Relative risk; CI: Confidence interval.

		Overall Survival		
	No. of Cases	**RR**	**95%CI**	**p-value**
Cytoplasmic ECD Expression				
negative/weak	**315**	**1**		
moderate/strong	**241**	**1.689**	**1.085-2.629**	**0.02**
Tumour stage				
postoperative pT2	**386**	**1**		
postoperative pT3	**170**	**3.126**	**1.899-5.146**	**0**
Gleason				
Score 2-6	**192**	**1**		
Score 7-10	**364**	**2.415**	**1.247-4.675**	**0.009**
R-status				
R0	**396**	**1**		
R1	**157**	**1.666**	**1.038-2.675**	**0.035**
Age				
≤60 Years	**194**	**1**		
>60 Years	**362**	**0.971**	**0.934-1.011**	**0.151**
PreOP PSA				
≤7.2ng/ml	**279**	**1**		
>7.2ng/ml	**269**	**1.529**	**0.965-2.425**	**0.071**

Table S2

Incidence of tumor formation in vector or ECD-overexpressing LNCaP xenograft model.

No. of Days	LNCaP Control group	ECD OE LNCaP Group
16	0 (0/26)/ 0%	6 (6/28)/ 21.4%
22	8 (8/26)/ 30.7%	20 (20/28)/ 71.4%
27	9 (9/26)/ 34.6%	23 (23/28)/ 82.1%
35	13 (13/26)/ 50%	26 (26/28)/ 92.8%

Table S3

List of ECD promoter mutants and the corresponding sequences deleted from TSS.

ECD Promotor Mutants	Sequence deleted from TSS
CS-HPRM35342-LvPG04-01- site-1Δ	698 bp – 682 bp
CS-HPRM35342-LvPG04-02-site-2Δ	657 bp – 641bp
CS-HPRM35342-LvPG04-03-site-3Δ	640 bp – 624 bp
CS- HPRM35342-LvPG04-04-site-1,2Δ	698 bp – 682 bp, 657 bp – 641bp
CS-HPRM35342-LvPG04-05-site-1,3Δ	698 bp – 682 bp, 640 bp – 624 bp
CS-HPRM35342- LvPG04-06 - site-2,3Δ	657 bp – 641bp, 640 bp – 624 bp
CS-HPRM35342-LvPG04-07 - site-1,2,3Δ	698 bp – 682 bp, 657 bp – 641bp, 640 bp – 624bp

Table S4

List of real time qRT-PCR primers of human genes.

Primer Name	Forward Sequence	Reverse Sequence
LDHA	TTGACCTACGTGGCTTGGAAG	GGTAACGGAATCGGGCTGAAT
HKII	GAGCCACCACTCACCCTACT	ACCCAAAGCACACACCGGAAGTT
PKM2	CCACTTGCAATTATTTGAGGAA	GTGAGCAGACCTGCCAGACT
ECD	ACTTTGAAACACACGAACCTGGCG	TGATGCAGGTGTGTGCTAGTTCCT
18S	GCTTAATTTGACTCAACACGGGA	AGCTATCAATCTGTCAATCCTGTC
AR	TTGCAAGAGAGCTGCATCAGT	ACTGTGTGTGGAAATAGATGGGC

Fig. S1

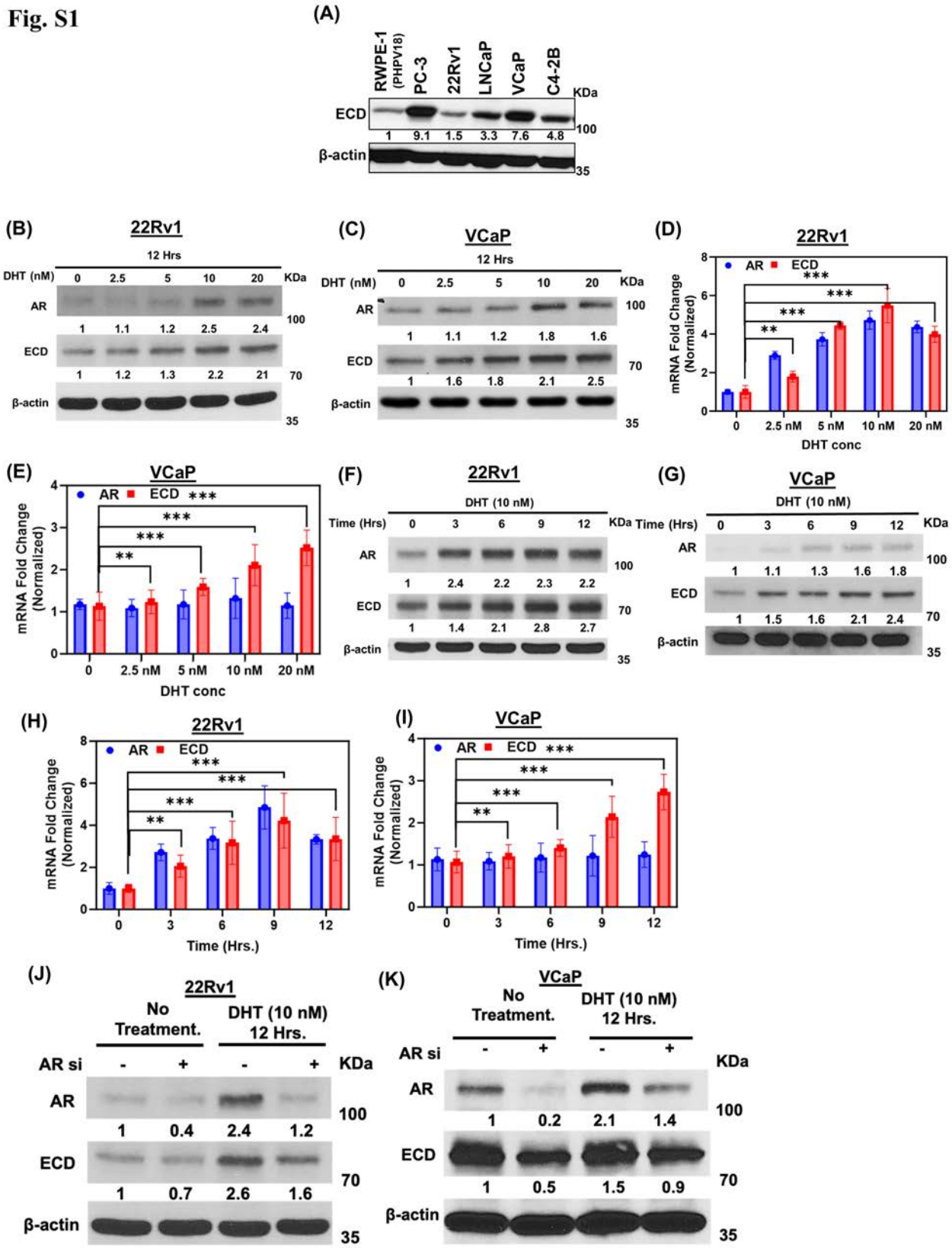
(A)
RWPE-1 (PHPV18)
PC-3
22Rv1
LNCaP
VCaP
C4-2B
KDa
ECD
1 9.1 1.5 3.3 7.6 4.8
100
β-actin
35
(B)
22Rv1
12 Hrs
DHT (nM) 0 2.5 5 10 20 KDa
AR
1 1.1 1.2 2.5 2.4
ECD
1 1.2 1.3 2.2 21
70
β-actin
35
(C)
VCaP
12 Hrs
DHT (nM) 0 2.5 5 10 20 KDa
AR
1 1.1 1.2 1.8 1.6
ECD
1 1.6 1.8 2.1 2.5
β-actin
(D)
22Rv1
AR ECD
mRNA Fold Change (Normalized)
0 2.5 nM 5 nM 10 nM 20 nM
DHT conc
(E)
VCaP
AR ECD
mRNA Fold Change (Normalized)
0 2.5 nM 5 nM 10 nM 20 nM
DHT conc
(F)
22Rv1
DHT (10 nM)
Time (Hrs) 0 3 6 9 12 KDa
AR
1 2.4 2.2 2.3 2.2
ECD
1 1.4 2.1 2.8 2.7
β-actin
(G)
VCaP
DHT (10 nM)
Time (Hrs) 0 3 6 9 12 KDa
AR
1 1.1 1.3 1.6 1.8
ECD
1 1.5 1.6 2.1 2.4
β-actin
(H)
22Rv1
AR ECD
mRNA Fold Change (Normalized)
Time (Hrs.)
(I)
VCaP
AR ECD
mRNA Fold Change (Normalized)
Time (Hrs.)
(J)
22Rv1
No Treatment.
DHT (10 nM) 12 Hrs.
AR si - + - + KDa
AR
1 0.4 2.4 1.2
ECD
1 0.7 2.6 1.6
β-actin
(K)
VCaP
No Treatment.
DHT (10 nM) 12 Hrs.
AR si - + - + KDa
AR
1 0.2 2.1 1.4
ECD
1 0.5 1.5 0.9
β-actin

Fig. S1. Higher expression of ECD in PC cell lines and AR regulates ECD expression in 22Rv1 and VCaP cells. **(A)** WB showing expression level of ECD in indicated PC cell lines in comparison to HPV18 immortalized epithelial cells. **(B & C)** 22Rv1 and VCaP cells were cultured in steroid free conditions for 72 hours. Cells were then treated with indicated concentrations of DHT for 12 hours and immunoblotted with anti-ECD or anti-AR antibodies. β- actin was used as a loading control. **(D & E)** qRT-PCR was performed in the same samples; RNA was isolated by standard TRIzol phenol chloroform method. 18s rRNA was used for normalization. **(F & G)** Similar protocols as mentioned above were used to perform a time response with DHT. Western blotting **(F & G)** and qRT-PCR **(H & I)** were performed on cell lysates, as above. **(J & K)** 22Rv1 and VCaP cell lines were transfected with control siRNA or AR siRNA and cultured for 72 hours. Cells were then treated with indicated concentrations of DHT for 12 hours and then lysates were western blotted with anti-ECD or anti-AR antibodies. β- actin was used as a loading control in all blots. Numbers below the blots show the quantification of band intensities after normalizing with their respective loading control, β- actin in comparison with control samples using ImageJ software. Bar graphs represent mean ± SEM from three independent experiments, each done in triplicates. Student t- test was used to calculate statistical significance *** $p < 0.001$, ** $p < 0.01$.

Fig. S2

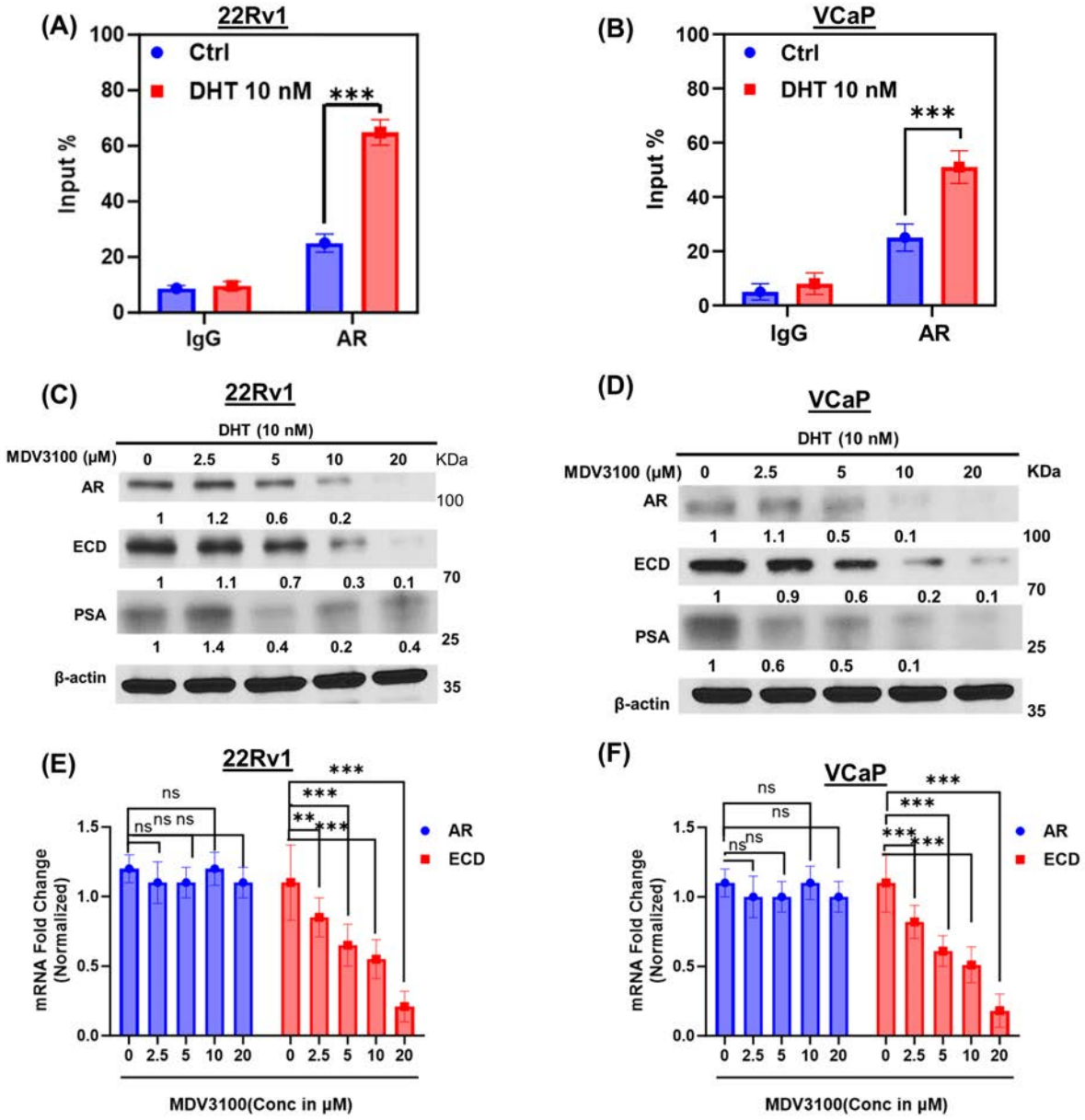
(A)
22Rv1
Ctrl
DHT 10 nM
***
Input %
IgG
AR
(B)
VCaP
Ctrl
DHT 10 nM
***
Input %
IgG
AR
(C)
22Rv1
DHT (10 nM)
MDV3100 (μM) 0 2.5 5 10 20 KDa
AR
1 1.2 0.6 0.2
ECD
1 1.1 0.7 0.3 0.1
PSA
1 1.4 0.4 0.2 0.4
β-actin
100
70
25
35
(D)
VCaP
DHT (10 nM)
MDV3100 (μM) 0 2.5 5 10 20 KDa
AR
1 1.1 0.5 0.1
ECD
1 0.9 0.6 0.2 0.1
PSA
1 0.6 0.5 0.1
β-actin
100
70
25
35
(E)
22Rv1
mRNA Fold Change (Normalized)
AR
ECD
MDV3100(Conc in μM)
(F)
VCaP
mRNA Fold Change (Normalized)
AR
ECD
MDV3100(Conc in μM)

Fig. S2. 22Rv1 and VCaP cells show increased AR occupancy on ECD promoter upon androgen treatment and Enzalutamide treatment decreases ECD expression. (A & B) Histograms showing relative pull-down enrichment ± SEM of ECD promotor by IgG and AR from three independent experiments as observed through chromatin immunoprecipitation (ChIP) analysis**.** Indicated cells were cultured in steroid-free conditions for 3 days, followed by dihydrotestosterone (DHT) treatment for 3 h. Cells were cross-linked with formaldehyde and chromatin was immunoprecipitated with antibody against AR or IgG, used as a non-binding Control. Immunoprecipitated DNA was quantified with qRT-PCR for specific binding sites at ECD promoter using primers encompassing all three sites -712 to -565 from transcription start site. Student t- test was performed to calculate statistical significance *** $p < 0.001$. **(C & D**) 22Rv1 and VCaP cell lines were cultured in steroid-free medium for 72 hours, cells were then treated with 10 nM DHT, followed by treatment with indicated concentration of MDV3100 for another 48 hours. Lysates were collected and western blotted with indicated antibodies. β-actin was used as a loading control. **(E & F)** qRT-PCR was performed in the same samples where the RNA was isolated by standard TRIzol phenol chloroform method. 18s rRNA was used for normalization. Bar graphs represent fold change ± SEM in AR and ECD mRNA in 22Rv1 **(E)** and VCaP cells **(F)** respect to vehicle treatment from three independent experiments. *Student t- test* was performed to calculate statistical significance *** $p < 0.001$, ** $p < 0.01$**.**

Fig. S3

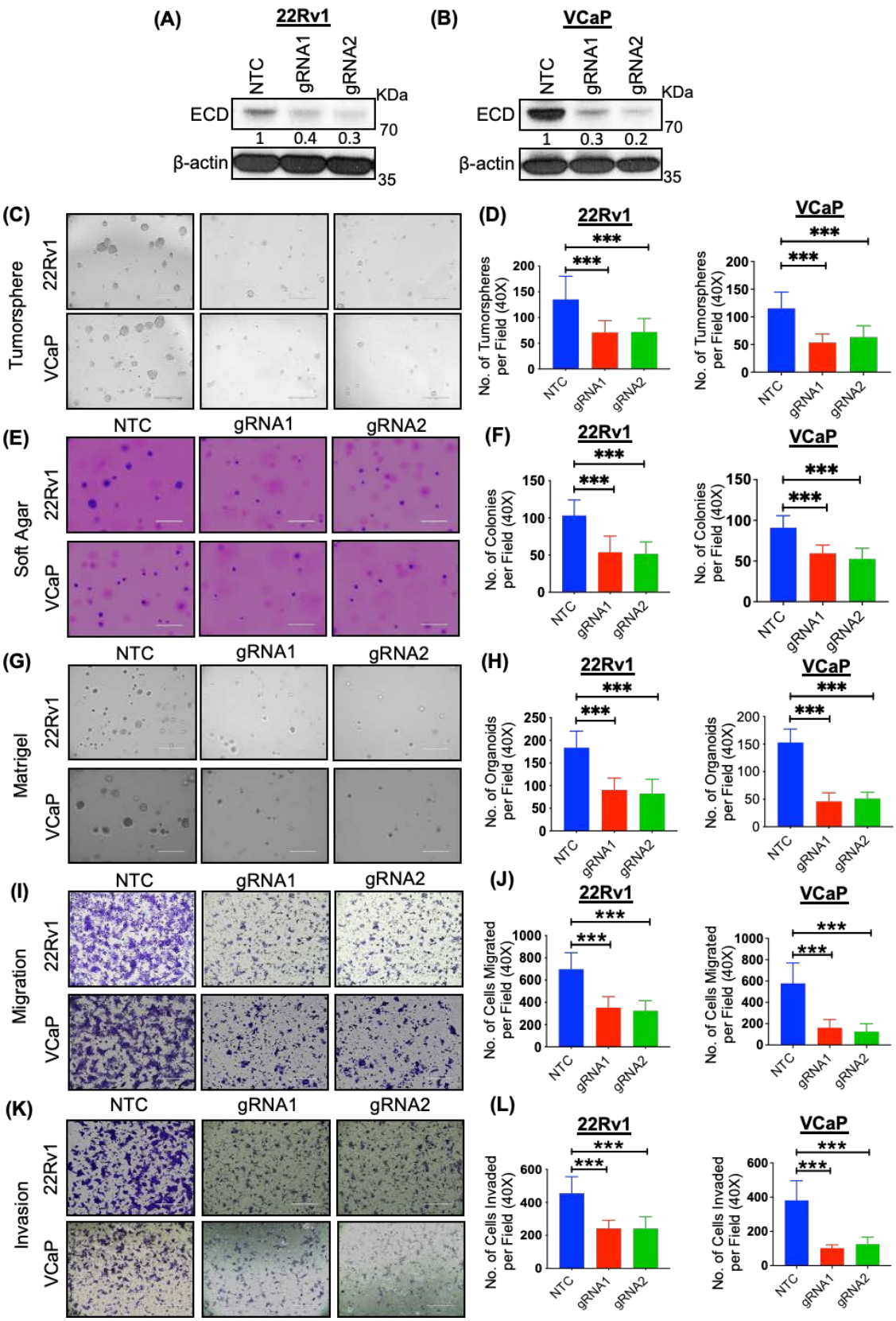
(A)
22Rv1
NTC
gRNA1
gRNA2
KDa
ECD
70
1
0.4
0.3
β-actin
35
(B)
VCaP
NTC
gRNA1
gRNA2
KDa
ECD
70
1
0.3
0.2
β-actin
35
(C)
Tumorsphere
22Rv1
VCaP
(D)
22Rv1
VCaP
No. of Tumorspheres per Field (40X)
NTC
gRNA1
gRNA2
***
(E)
Soft Agar
22Rv1
VCaP
NTC
gRNA1
gRNA2
(F)
No. of Colonies per Field (40X)
(G)
Matrigel
(H)
No. of Organoids per Field (40X)
(I)
Migration
(J)
No. of Cells Migrated per Field (40X)
(K)
Invasion
(L)
No. of Cells Invaded per Field (40X)

Fig. S3. ECD depletion diminishes oncogenic traits in 22Rv1 and VCaP prostate cancer cells. 22Rv1 and VCaP cells expressing doxycycline (Dox) regulated Cas9 and guide RNAs targeting either ECD (gRNA1 & 2) or non-targeting control (NTC) were cultured in the presence of Dox (1 μg/ml) for 96 hours to deplete ECD. **(A & B)** Western blot depicting expression of ECD in 22Rv1 **(A)** and VCaP **(B)** post Dox (1 μg/ml) treatment for 96 hours. Numbers below the blot show the quantification of band intensities after normalizing with their respective loading control β-actin in comparison with NTC, using ImageJ software. Representative images and histograms depicting tumorsphere **(C & D),** soft agar colony **(E & F**), Matrigel organoid formation **(G & H),** migration **(I & J),** and invasion **(K & L),** of control and ECD depleted 22Rv1 and VCaP cells. The representative images of tumorspheres, soft agar colonies, Matrigel organoids, migration and invasion are at100 x magnification, scale bar, 400 μm. The Bar graph data presented as mean values ± SEM of three experiments, each done in triplicates. *Student t-test* was used to calculate statistical significance *** $p < 0.001$.

Fig. S4

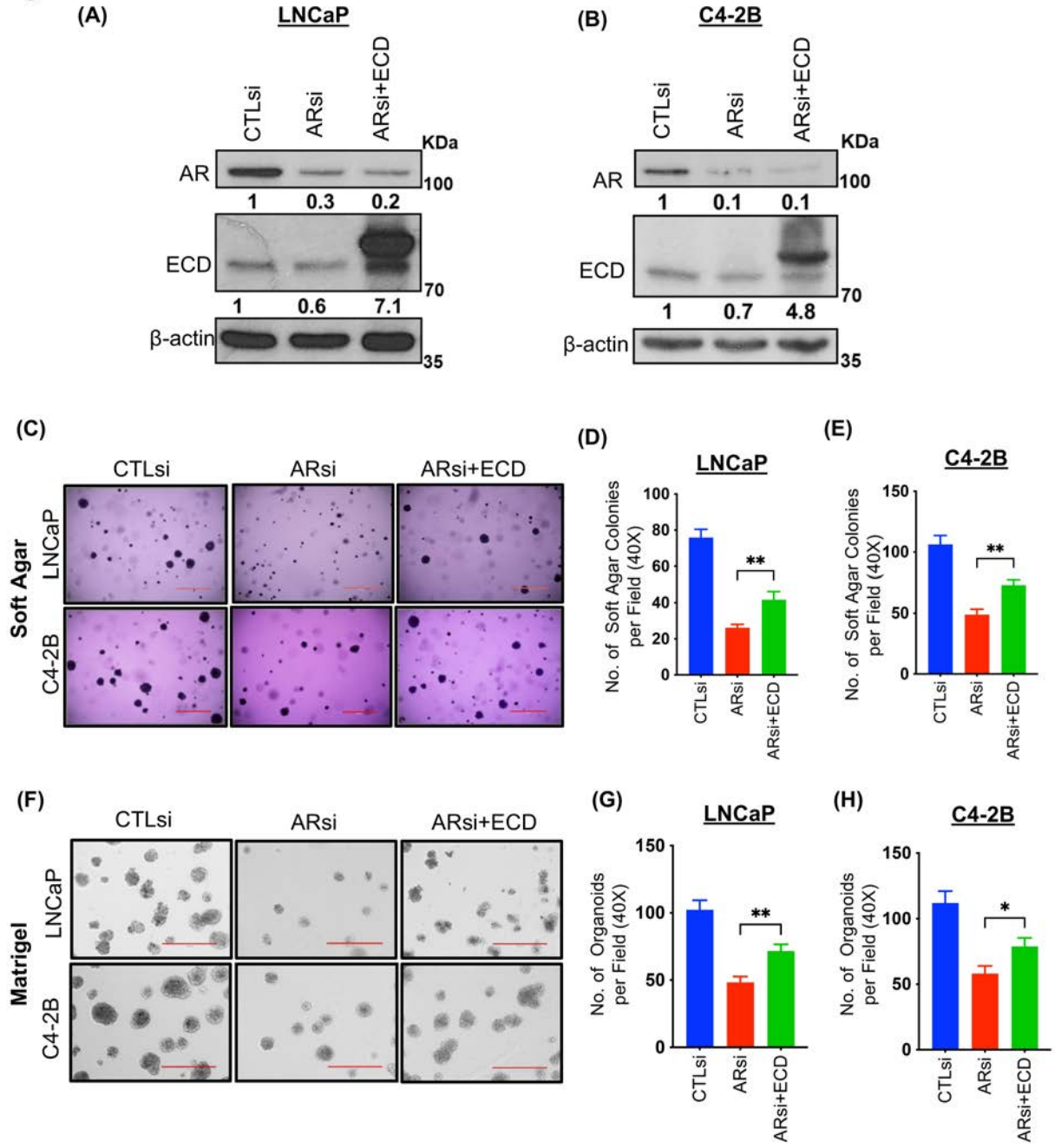
(A)
LNCaP
CTLsi
ARsi
ARsi+ECD
KDa
AR
100
1
0.3
0.2
ECD
70
1
0.6
7.1
β-actin
35
(B)
C4-2B
CTLsi
ARsi
ARsi+ECD
KDa
AR
100
1
0.1
0.1
ECD
70
1
0.7
4.8
β-actin
35
(C)
CTLsi
ARsi
ARsi+ECD
Soft Agar
LNCaP
C4-2B
(D)
LNCaP
No. of Soft Agar Colonies per Field (40X)
100
80
60
40
20
0
**
CTLsi
ARsi
ARsi+ECD
(E)
C4-2B
No. of Soft Agar Colonies per Field (40X)
150
100
50
0
**
CTLsi
ARsi
ARsi+ECD
(F)
CTLsi
ARsi
ARsi+ECD
Matrigel
LNCaP
C4-2B
(G)
LNCaP
No. of Organoids per Field (40X)
150
100
50
0
**
CTLsi
ARsi
ARsi+ECD
(H)
C4-2B
No. of Organoids per Field (40X)
150
100
50
0
*
CTLsi
ARsi
ARsi+ECD

Fig. S4. ECD overexpression partially rescues detrimental effect of AR knockdown of PC cells. LNCaP and C4-2B cells were transfected with AR siRNA and rescued with ECD overexpression. Cell lysates were collected 96 hours post transfection. **(A & B)** Western blot depicting expression of AR and ECD post AR knockdown. Numbers below the blot show the quantification of band intensities after normalizing with their respective loading control, β- actin in comparison with vector control using ImageJ software. Representative images and histograms depicting soft agar colony **(C-E**) and Matrigel organoid formation **(F-H),** of LNCaP and C4-2B post AR knockdown and ECD rescued cells. The representative images of soft agar colonies and Matrigel organoids are at 100x magnification, scale bar, 400 µm. Bar graphs show mean values ± SEM of three experiments done in triplicates from 40x magnification images. *Student t-test* was used to calculate statistical significance ** $p < 0.01$, * $p < 0.05$.

Fig. S5

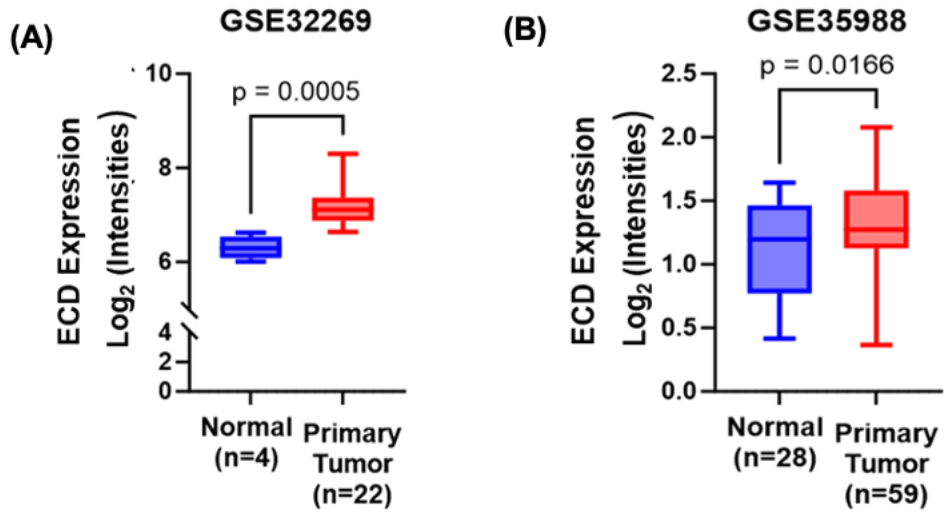

Fig. S5. PC tissue specimens show higher expression of *ECD* mRNA. Box plot showing mRNA expression of *ECD* from **(A)** 4 normal and 22 tumor samples from cohort 1 (GSE32269) and **(B)** 28 normal and 59 tumor samples from another independent cohort (GSE35988). The mentioned two publicly available datasets were analyzed for *ECD* mRNA expression. A *paired t* test was used to compare expression in normal versus cancer samples.

Fig. S6

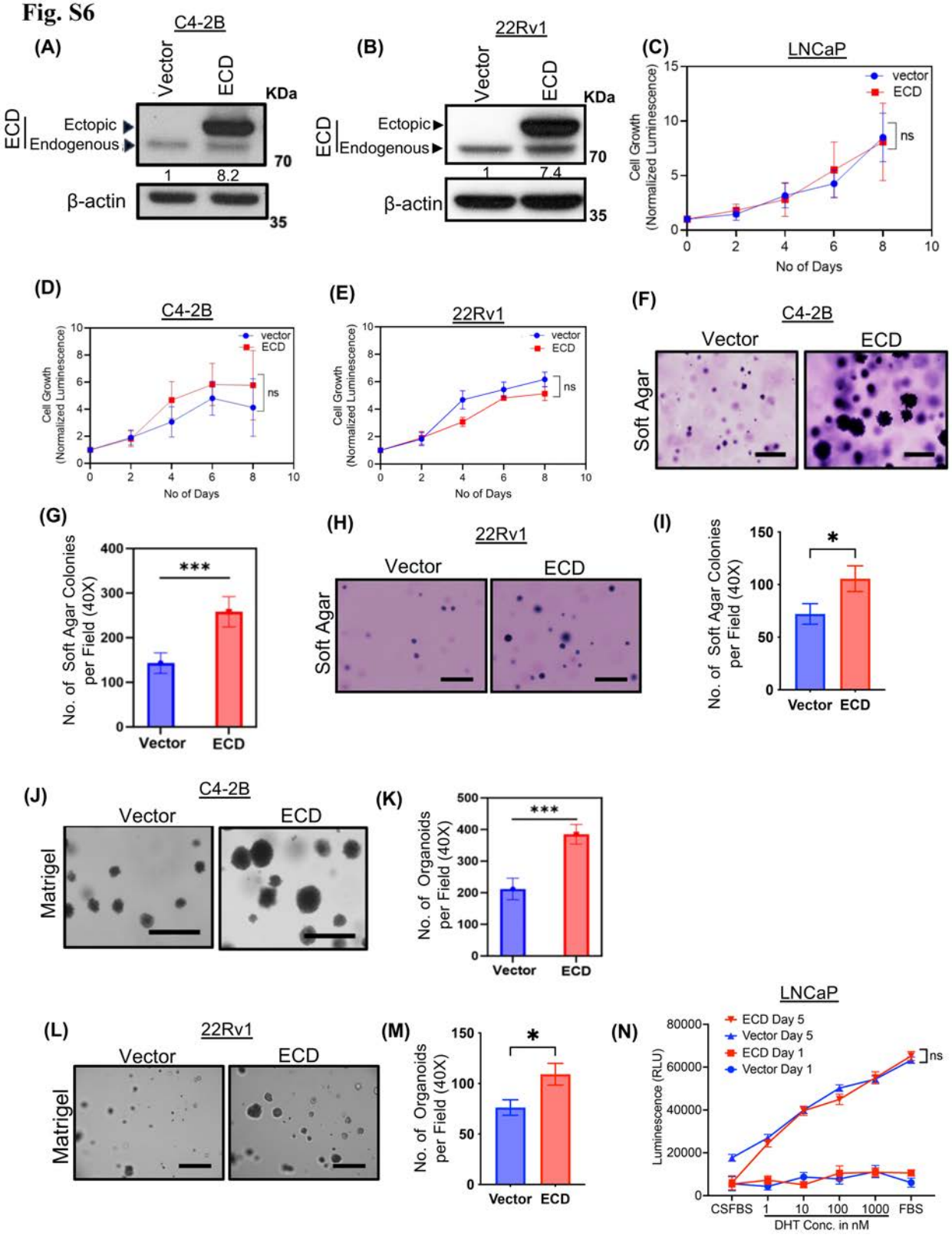
(A)
C4-2B
Vector
ECD
KDa
ECD
Ectopic
Endogenous
70
1
8.2
β-actin
35
(B)
22Rv1
Vector
ECD
KDa
ECD
Ectopic
Endogenous
70
1
7.4
β-actin
35
(C)
LNCaP
vector
ECD
ns
Cell Growth (Normalized Luminescence)
No of Days
(D)
C4-2B
vector
ECD
ns
Cell Growth (Normalized Luminescence)
No of Days
(E)
22Rv1
vector
ECD
ns
Cell Growth (Normalized Luminescence)
No of Days
(F)
C4-2B
Vector
ECD
Soft Agar
(G)
***
No. of Soft Agar Colonies per Field (40X)
Vector
ECD
(H)
22Rv1
Vector
ECD
Soft Agar
(I)
*
No. of Soft Agar Colonies per Field (40X)
Vector
ECD
(J)
C4-2B
Vector
ECD
Matrigel
(K)
***
No. of Organoids per Field (40X)
Vector
ECD
(L)
22Rv1
Vector
ECD
Matrigel
(M)
*
No. of Organoids per Field (40X)
Vector
ECD
(N)
LNCaP
ECD Day 5
Vector Day 5
ECD Day 1
Vector Day 1
ns
Luminescence (RLU)
CSFBS
1
10
100
1000
FBS
DHT Conc. in nM

Fig. S6. ECD-overexpressing PC cells exhibit enhanced anchorage independence and Matrigel three-dimensional (3D) growth but show no alteration in 2-D proliferation rate or Androgen dependence. (A & B) Western blot shows overexpression of ECD in C4-2B **(A)** and 22Rv1 **(B)** cell lines. Numbers below the blot shows the quantification of band intensities after normalizing with their respective loading control, β- actin in comparison with vector cells using ImageJ software. **(C-E)** Cell proliferation curves showing proliferation rate of LNCaP **(C),** C4-2B **(D)** and 22Rv1 **(E)** cells overexpressing ECD. Assays were performed using Cell-Titer-Glo**.** Luminescence values were plotted against number of days and normalized to day 1. Quantitation data represents mean ± SEM with two-way ANOVA test. $n = 3$; ns, $P > 0.05$. **(F & H)** Representative images in 100x magnification (scale bar, 400 μm) depict soft agar colony formation abilities upon overexpression of ECD in C4-2B **(F)** and 22Rv1 **(H)** cells. Images were taken after fixing and staining the colonies with 0.05% crystal violet. **(G & I)** Bars depict the mean ± SEM of soft agar colonies number per 40x magnification field in vector and ECD overexpressing C4-2B **(G)** and 22Rv1 **(I)** cells. Data represent three independent experiments, each done in triplicates. ***$p < 0.001$, *$p < 0.05$. Student t-test was used to calculate statistical significance. **(J & L)** Representative images in 100x magnification (scale bar, 400 μm) depict 3D colony formation abilities of C4-2B **(J)** and 22Rv1 **(L)** cells in Matrigel upon overexpression of ECD. **(K & M)** Bar graphs show mean ± SEM of 3D colonies number per 40x magnification field in vector and ECD overexpressing C4-2B **(K)** and 22Rv1 **(M)** cells. Data represent three independent experiments, each done in triplicates. ***$p < 0.001$, *$p < 0.05$. Student t-test was used to calculate statistical significance. **(N)** LNCaP cells expressing vector or ECD were cultured in charcoal-stripped serum containing phenol red free medium for 72 hours. Cells were then treated with indicated concentrations of DHT. Growth Assays were performed using Cell-Titer-Glo**.** Luminescence

values were plotted for both Day 1 and Day 5. Data represent three independent experiments, each done in triplicates. $^{ns}p > 0.05$, Two-way ANOVA (mixed model) was used to calculate statistical significance.

Fig. S7

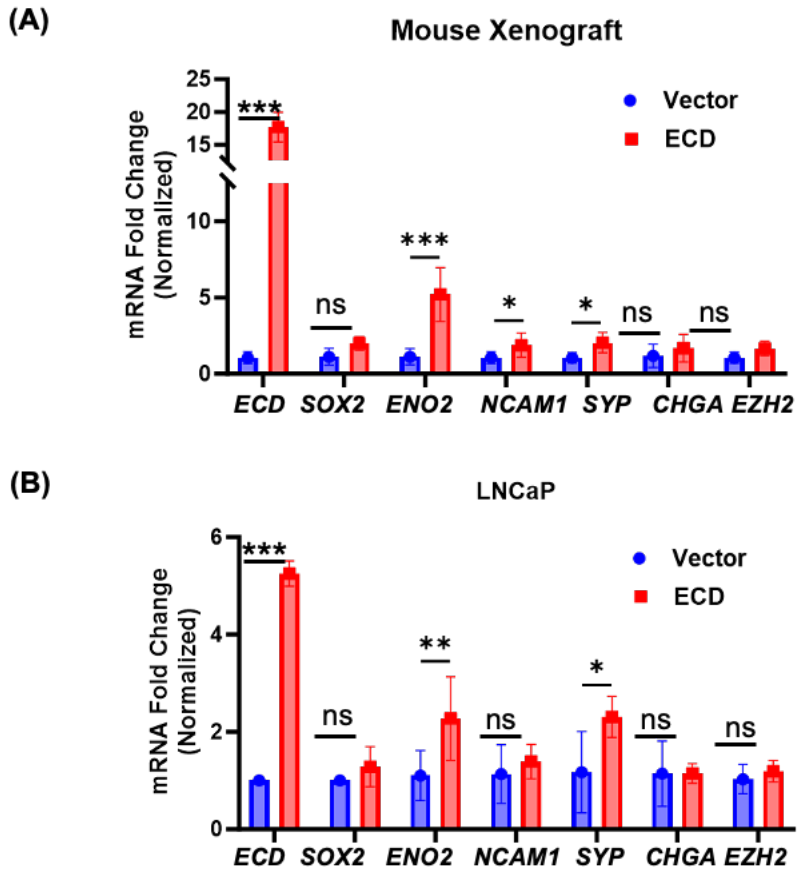

Fig. S7. Transcriptomic analysis of ECD overexpressing prostate xenograft tumors and LNCaP cell line confirm upregulation of Neuroendocrine PC markers. (A & B) qRT-PCR analysis of indicated neuroendocrine (NE) signature genes of LNCaP-vector expressing and LNCaP ECD-OE xenograft tumors **(A)** and vector expressing or ECD-OE LNCaP cells **(B).** 18s rRNA was used for normalization. mRNA quantitation data represents mean ± SEM with two-tailed unpaired *t* test. $n = 3$; ns, $P > 0.05$, **, $P < 0.01$; ***, $P < 0.001$.

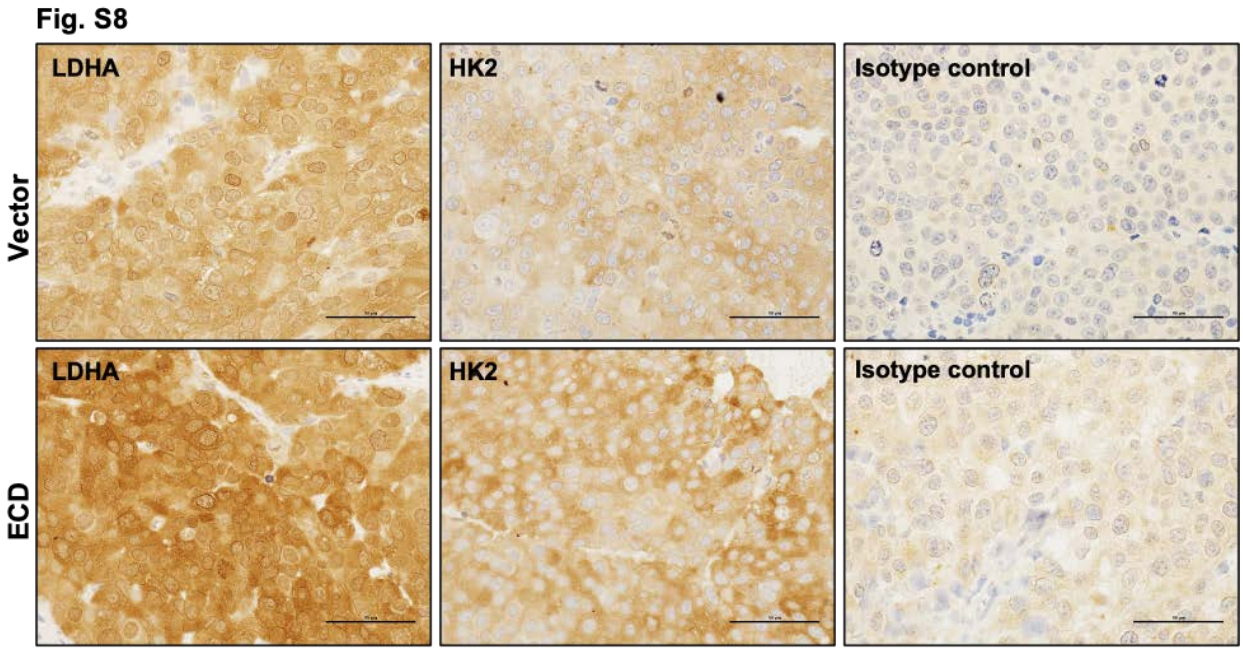

Fig. S8. Increased expression of glycolytic enzymes, LDHA and HK2 in ECD overexpressing LNCaP tumors. IHC analysis of paraffin embedded sections of LNCaP xenografts tumors from vector group and ECD-overexpressing groups with LDHA and HK2. Rabbit IgG was used as isotype control for the staining. Representative images from both groups, in 400x magnification (scale bar, 50 μm).

Fig. S9

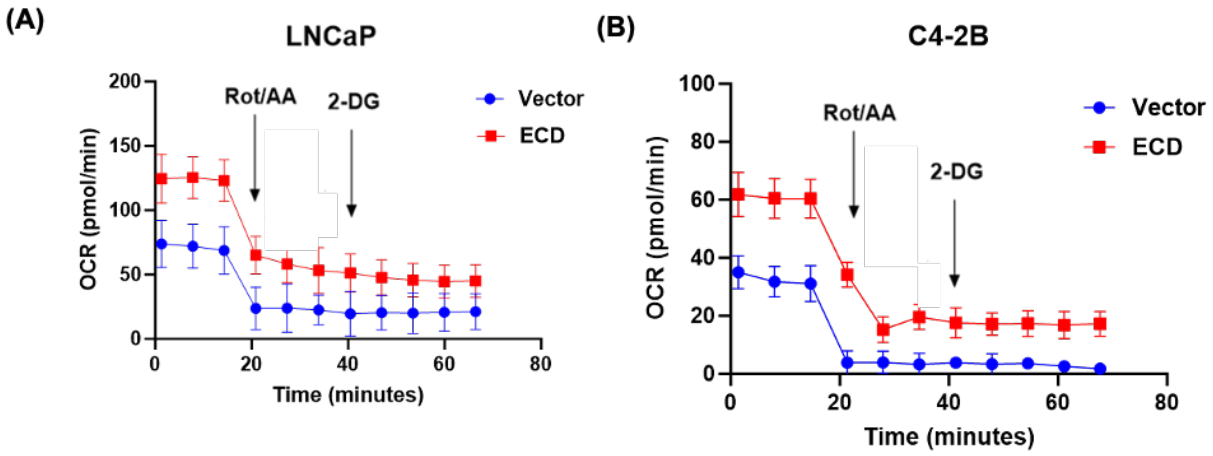

Fig. S9. Seahorse Glycolytic Rate assay in prostate cancer cell lines overexpressing ECD. **(A & B)** Oxygen consumption rates (OCR) at various time points followed by injections of Rot/AA (0.5 μM), and 2-DG (50 mM) in vector or ECD-OE cells.

Fig. S10

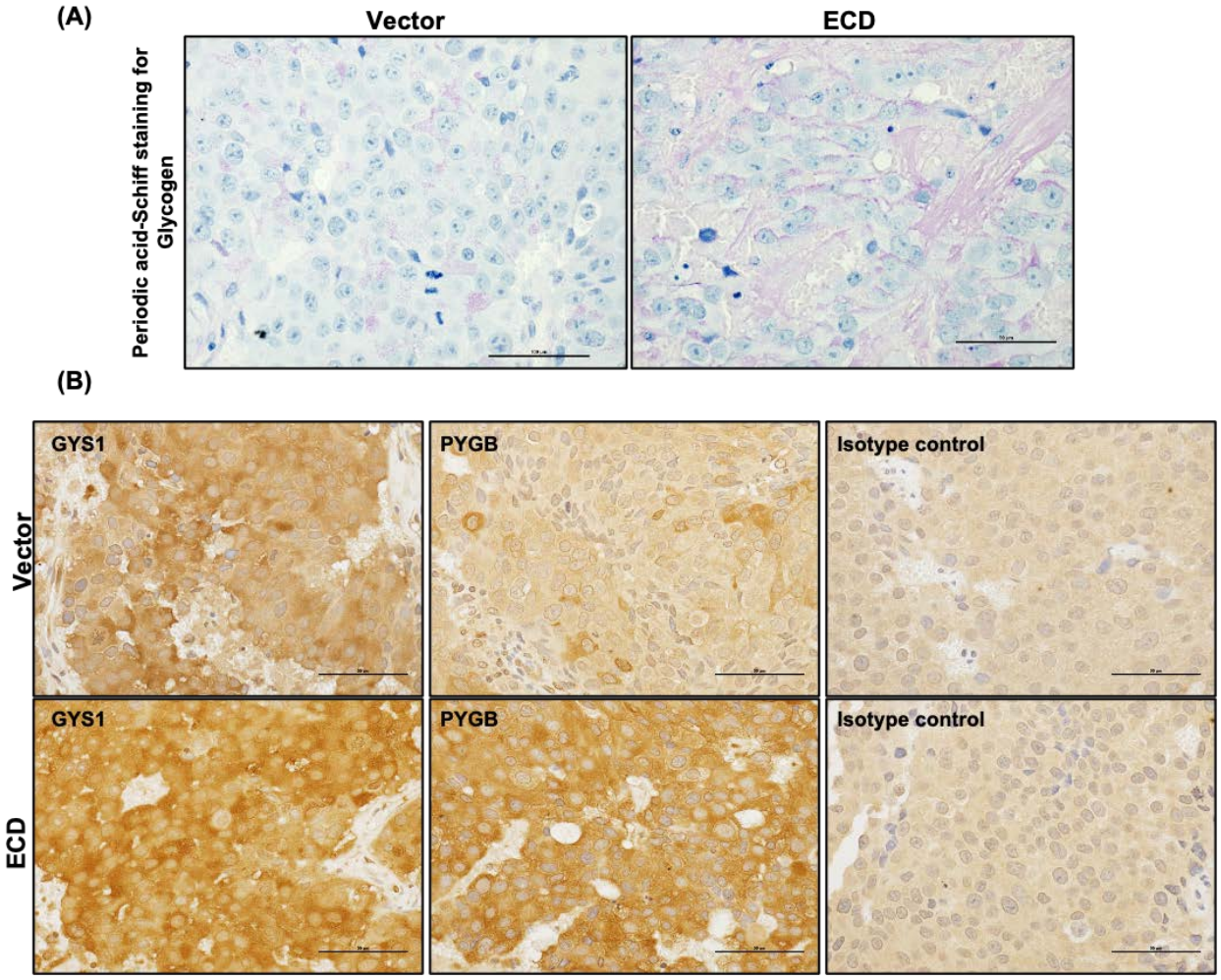

Fig. S10. Enhanced glycogenesis and glycogen metabolism in ECD overexpressing LNCaP tumors. (A) Periodic acid-Schiff staining shows increased glycogen deposition represented by magenta staining in ECD overexpressing tumors compared to vector expressing tumors. (**B**) IHC analysis of paraffin embedded sections of LNCaP xenografts tumors from vector group and ECD-overexpressing groups with glycogen synthase 1 (GYS1) and glycogen phosphorylase, brain (PYGB). Rabbit IgG was used as isotype control for the staining. Representative images from both groups, in 400x magnification (scale bar, 50 µm).